Astronomy
&
Astrophysics

The influence of chemical composition on the properties of Cepheid stars

II. The iron content[*],[**]

M. Romaniello[1], F. Primas[1], M. Mottini[1], S. Pedicelli[1,2], B. Lemasle[3], G. Bono[1,2,4], P. François[5], M. A. T. Groenewegen[6], and C. D. Laney[7]

[1] European Southern Observatory, Karl-Schwarzschild-Strasse 2, 85748 Garching bei München, Germany
    e-mail: bono@mporzio.astro.it
[2] Università of Roma Tor Vergata, Department of Physics, via della Ricerca Scientifica 1, 00133 Roma, Italy
[3] Université de Picardie Jules Verne, Faculté des Sciences, 33 rue Saint-Leu, 80039 Amiens Cedex 1, France
[4] INAF - Osservatorio Astronomico di Roma, via Frascati 33, 00040 Monte Porzio Catone, Italy
[5] Observatoire de Paris-Meudon, GEPI, 61 avenue de l'Observatoire, 75014 Paris, France
[6] Royal Observatory of Belgium, Ringlaan 3, 1180 Brussels, Belgium
[7] South African Astronomical Observatory, PO Box 9, 7935 Observatory, South Africa

ABSTRACT

Context. The Cepheid period-luminosity (PL) relation is unquestionably one of the most powerful tools at our disposal for determining the extragalactic distance scale. While significant progress has been made in the past few years towards its understanding and characterization both on the observational and theoretical sides, the debate on the influence that chemical composition may have on the PL relation is still unsettled.
Aims. With the aim to assess the influence of the stellar iron content on the PL relation in the V and K bands, we have related the V-band and the K-band residuals from the standard PL relations of Freedman et al. (2001, ApJ, 553, 47) and Persson et al. (2004, AJ, 128, 2239), respectively, to [Fe/H].
Methods. We used direct measurements of the iron abundances of 68 Galactic and Magellanic Cepheids from FEROS and UVES high-resolution and high signal-to-noise spectra.
Results. We find a mean iron abundance ([Fe/H]) about solar ($\sigma = 0.10$) for our Galactic sample (32 stars), ~ -0.33 dex ($\sigma = 0.13$) for the Large Magellanic Cloud (LMC) sample (22 stars) and ~ -0.75 dex ($\sigma = 0.08$) for the Small Magellanic Cloud (SMC) sample (14 stars). Our abundance measurements of the Magellanic Cepheids double the number of stars studied up to now at high resolution. The metallicity affects the V-band Cepheid PL relation and metal-rich Cepheids appear to be systematically fainter than metal-poor ones. These findings depend neither on the adopted distance scale for Galactic Cepheids nor on the adopted LMC distance modulus. Current data do not allow us to reach a firm conclusion concerning the metallicity dependence of the K-band PL relation. The new Galactic distances indicate a small effect, whereas the old ones support a marginal effect.
Conclusions. Recent robust estimates of the LMC distance and current results indicate that the Cepheid PL relation is not Universal.

Key words. stars: abundances – stars: distances – stars: variables: Cepheids

1. Introduction

Since the dawn of modern astronomy the Cepheid Period-Luminosity (PL) relation is a key tool in determining Galactic and extragalactic distances. In spite of its fundamental importance, the debate on the role played by the chemical composition on the pulsation properties of Cepheids is still open, with different theoretical models and observational results leading to markedly different conclusions.

From the theoretical point of view pulsation models by different groups lead to substantially different results. Linear models (e.g. Chiosi et al. 1992; Sandage et al. 1999; Baraffe & Alibert 2001), based on nonadiabatic radiative models, suggest a moderate dependence of the PL relation on the metallicity.

The predicted change at $\log(P) = 1$ is less than 0.1 mag for metal abundances ranging from the SMC ($Z = 0.004$) to the Galaxy ($Z = 0.02$), independent of wavelength. Nonlinear convective models (e.g. Bono et al. 1999; Caputo et al. 2000; Caputo 2008) instead predict a larger dependence on the same interval of metallicity: the change is 0.4 mag in V, 0.3 mag in I and 0.2 mag in K, again at $\log(P) = 1$. Moreover, the predicted change in these latter models is such that metal-rich Cepheids are fainter than metal-poor ones, at variance with the results of the linear models. Fiorentino et al. (2002) and, more recently, Marconi et al. (2005) investigations, also based on nonlinear models, suggest that there may be also a dependence on the helium abundance.

On the observational side, the majority of the constraints comes from indirect measurements of the metallicity, mostly in external galaxies, such as oxygen nebular abundances derived from spectra of H II regions at the same Galactocentric distance as the Cepheid fields (e.g. Sasselov et al. 1997;

Table 1. Overview of recent results for the metallicity sensitivity of Cepheid distances. In the first column is listed the variation of the distance modulus μ per dex of metallicity, the negative sign indicates that the true distance is longer than the one obtained neglecting the effect of the metallicity. In the second column is listed the elemental abundance used as reference for the metallicity. The third and fourth columns give the method and the reference of the different studies. See also Fig. 1.

$\delta\mu/\delta$[M/H] (mag/dex)		Method	Reference
-0.32 ± 0.21	[Fe/H]	Analysis of Cepheids in 3 fields of M 31 (*BVRI* bands)	Freedman & Madore (1990)
-0.88 ± 0.16	[Fe/H]	Comparison of Cepheids from 3 fields of M 31 and LMC (*BVRI* bands)	Gould (1994)
-0.40 ± 0.20	[O/H]	Simultaneous solution for distances to 17 galaxies (*UBVRIJHK* bands)	Kochanek (1997)
$-0.44^{+0.10}_{-0.20}$	[O/H]	Comparison of EROS observations of SMC and LMC Cepheids (*VR* bands)	Sasselov et al. (1997)
-0.24 ± 0.16	[O/H]	Comparison of HST observations of inner and outer fields of M 101	Kennicutt et al. (1998)
-0.12 ± 0.08	[O/H]	Comparison of 10 Cepheid galaxies with Tip of the Red Giant Branch distances	Kennicutt et al. (1998)
-0.20 ± 0.20	[O/H]	Value adopted for the HST Key Project final result	Freedman et al. (2001)
0	[Fe/H]	OGLE result comparing Cepheids in IC 1613 and MC (*VI* bands)	Udalski et al. (2001)
0	[O/H]	Comparison of Planetary Nebula luminosity function distance scale and Surface Brightness fluctuation distance scale	Ciardullo et al. (2002)
-0.24 ± 0.05	[O/H]	Comparison of 17 Cepheid galaxies with Tip of the Red Giant Branch distances	Sakai et al. (2004)
-0.21 ± 0.19	[Fe/H]	Baade-Wesselink analysis of Galactic and SMC Cepheids (*VK* bands)	Storm et al. (2004)
-0.23 ± 0.19	[Fe/H]	Baade-Wesselink analysis of Galactic and SMC Cepheids (*I* band)	Storm et al. (2004)
-0.29 ± 0.19	[Fe/H]	Baade-Wesselink analysis of Galactic and SMC Cepheids (*W* index)	Storm et al. (2004)
-0.27 ± 0.08	[Fe/H]	Compilation from the literature of distances and metallicities of 53 Galactic and MC Cepheids (*VIWK* bands)	Groenewegen et al. (2004)
-0.39 ± 0.03	[Fe/H]	Cepheid distances to SNe Ia host galaxies	Saha et al. (2006)
-0.29 ± 0.09	[O/H]	Cepheids in NGC 4258 and [O/H] gradient from Zaritsky et al. (1994)	Macri et al. (2006)
-0.10 ± 0.03	[Fe/H]	Weighted mean of Kennicutt, Macri and Groenewegen estimates	Benedict et al. (2007)
-0.017 ± 0.113	[O/H]	Comparison between Cepheid and TRGB distances for 18 galaxies	Tammann et al. (2007)
0	[Fe/H]	Comparison between the slopes of Galactic and LMC Cepheids	Fouqué et al. (2007)
$+0.05 \pm 0.03$	[Fe/H]	Predicted Period-Wesenheit (*V, I*) relation	Bono et al. (2008)

Kennicutt et al. 1998; Sakai et al. 2004). These analyses indicate that metal-rich Cepheids are brighter than metal-poor ones (hence at variance with the predictions of nonlinear convective models), but it is important to note that the results span a disappointingly large range of values (see Table 1 and Fig. 1).

More recently Macri et al. (2006) found, by adopting a large sample of Cepheids in two different fields of NGC 4258 and the [O/H] gradient based on H II regions provided by Zaritsky et al. (1994), a metallicity effect of $\gamma = -0.29 \pm 0.09$ mag/dex. This galaxy has been adopted as a benchmark for estimating the metallicity effect, since an accurate geometrical distance based on water maser emission is available (Herrnstein et al. 2005). However, in a thorough investigation Tammann et al. (2007) suggested that the flat slope of the Period-Color relation of the Cepheids located in the inner metal-rich field could be due to a second parameter, likely helium, other than the metal abundance. Furthermore, Bono et al. (2008) found, using the new and more accurate nebular oxygen abundances for a good sample of H II region in NGC 4258 provided by Dìaz et al. (2000), a shallower abundance gradient. In particular, the new estimates seem to suggest that both the inner and the outer field might have a mean oxygen abundance very similar to LMC. They also found a very good agreement between predicted and observed Period-Wesenheit (*V, I*) relation. Nonlinear convective models predict for this relation a metallicity effect of $\gamma = +0.05 \pm 0.03$ mag/dex.

On the basis of independent distances for 18 galaxies based on Cepheid and on the Tip of the Red Giant Branch, Tammann et al. (2007) found a small metallicity effect ($\gamma = -0.017 \pm 0.113$ mag/dex). On the other hand, Fouqué et al. (2007) using a sample of 59 Galactic Cepheids whose distances were estimated using different methods – HST trigonometric

parallaxes (Benedict et al. 2007), revised Hipparcos parallaxes (van Leeuwen et al. 2007), infrared surface brightness method (Fouqué & Gieren 1997), and interferometric Baade-Wesselink method (Kervella et al. 2004), zero-age-main-sequence fitting of open clusters (Turner & Burke 2002) – found no significant difference between optical and Near-Infrared (NIR) slopes of Galactic and LMC Cepheids (Udalski et al. 1999; Persson et al. 2004).

An alternative approach is to measure directly the metal content of Cepheid stars, which, so far, has been attempted only by few studies, primarily focused on stars of our own Galaxy (Luck & Lambert 1992; Fry & Carney 1997; Luck et al. 1998; Andrievsky et al. 2002a,b,c; Luck et al. 2003; Andrievsky et al. 2004). Fry & Carney (1997, hereafter FC97), for instance, have derived iron and α-element abundances for 23 Galactic Cepheids from high resolution and high signal-to-noise spectra. They found a spread in [Fe/H] of about 0.4 dex, which they claim is real. Using approximately half of their sample, the stars belonging to clusters or associations, they have made a preliminary evaluation of metallicity effects on the zero point of the PL relation, finding that metal-rich Cepheids are brighter than metal-poor ones. Thus, finding a result similar to the studies based on indirect measurements of the metallicity.

The impressive observational effort carried out by Andrievsky and collaborators (Andrievsky et al. 2002a,b,c; Luck et al. 2003; Andrievsky et al. 2004; Kovtyukh et al. 2005b) has, instead, taken advantage of high resolution spectra of 130 Galactic Cepheids (collected with different instruments at different telescopes) in order to determine their chemical composition and study the Galactic abundance gradient. The sample covers a range of Galactocentric distances from 4
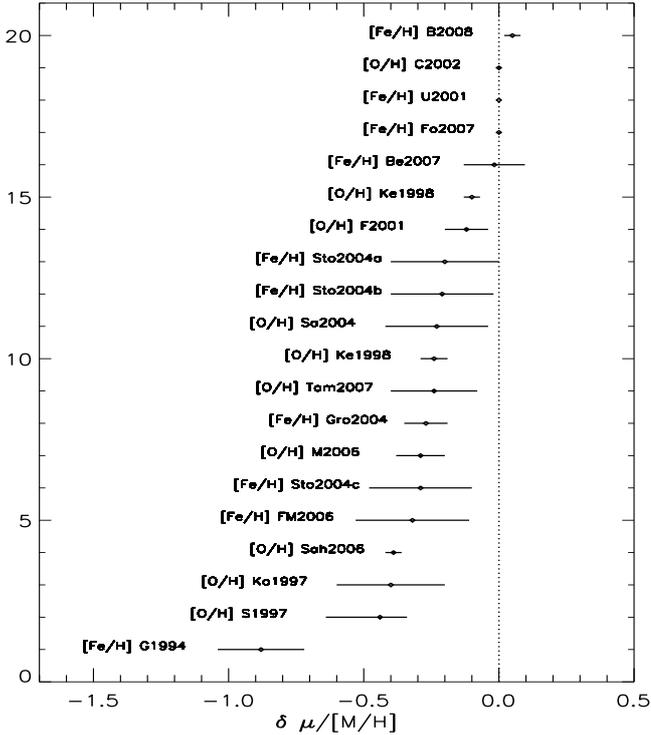
Fig. 1. Comparison of recent results for the metallicity sensitivity of Cepheid distances. FM1990: Freedman & Madore (1990); G1994: Gould (1994); Ko1997: Kochanek (1997); S1997: Sasselov et al. (1997); Ke1998: Kennicutt et al. (1998); F2001: Freedman et al. (2001); U2001: Udalski et al. (2001); C2002: Ciardullo et al. (2002); Sa2004: Sakai et al. (2004); Sto2004: Storm et al. (2004); Gro2004: Groenewegen et al. (2004); M2006: Macri et al. (2006); Sah2006: Saha et al. (2006); Be2007: Benedict et al. (2007); Fo2007: Fouqué et al. (2007); Tam2007: Tammann et al. (2007); B2008: Bono et al. (2008). See Table 1.

to 14 kpc. The emerging picture can be best described by a relatively steep gradient (about -0.14 dex kpc^{-1}) for Galactocentric distances less than 7 kpc, followed by a much shallower slope (≈ -0.03 dex kpc^{-1}) between 7 and 10 kpc, a discontinuity at approximately 10 kpc and a nearly constant metallicity of about -0.2 dex towards larger Galactocentric distances, out to about 14 kpc. In relation to our work, it is important to note that Andrievsky and collaborators did not investigate the effects of the chemical composition on the Cepheid PL relation: on the contrary, they used the PL relation to determine the distances of their stars.

Outside our Galaxy, Luck & Lambert (1992, hereafter LL92) have studied 10 Cepheids in the Magellanic Clouds (MCs). Five are in the Large MC (LMC) and five in the Small MC (SMC). For the former sample, they found a mean [Fe/H] of -0.36 dex with a dispersion of 0.3 dex, while for the latter one the mean [Fe/H] is -0.60 dex with a rather small dispersion of less than 0.15 dex. A more recent study by Luck et al. (1998, hereafter L98) on 10 LMC Cepheids and 6 SMC Cepheids, 4 of which in common with LL92, confirmed the mean [Fe/H] value in the LMC (-0.30 dex), found very little evidence of a significant metallicity dispersion in the LMC (contrary to LL92, but similarly to the SMC), and slightly revised downwards the mean [Fe/H] of the SMC (-0.74 vs. -0.60 found by LL92).

Finally, we mention two studies that followed slightly different approaches. Groenewegen et al. (2004) have selected from the literature a sample of 37 Galactic, 10 LMC and 6 SMC

Cepheids for which individual metallicity estimates and *BVIK* photometry were known. Their work aimed at investigating the metallicity dependence of the PL relation using individual metallicity determinations as well as good individual distance estimates for Galactic Cepheids. They inferred a metallicity effect of about -0.27 ± 0.08 mag/dex in the zero point in *VIWK*, in the sense that metal-rich Cepheids are brighter than the metal-poor ones (see Table 1 and Fig. 1, for a comparison with other studies). Also Storm et al. (2004) discussed the effect of the metallicity on the PL relation using 34 Galactic and 5 SMC Cepheids, for which they determined accurate individual distances with the Baade-Wesselink method. Assuming an average abundance for the SMC Cepheids of [Fe/H] = -0.7 and solar metallicity for the Galactic ones, they determined, in a purely differential way, the following corrections: -0.21 ± 0.19 for the *V* and *K* bands, -0.23 ± 0.19 for the *I*-band and -0.29 ± 0.19 for the Wesenheit index W. These agree well with Groenewegen et al. (2004).

Despite these ongoing observational efforts, it is important to underline that none of the observational studies undertaken so far has directly determined elemental abundances of a large sample of Cepheids in order to explicitly infer the metallicity effect on the PL relation, taking advantage of a sample that has been homogeneously analysed.

The novelty of our approach consists exactly in this, i.e. in the homogeneous analysis of a large sample of stars (68) in three galaxies (the Milky Way, the LMC and the SMC) spanning a factor of ten in metallicity and for which distances and *BVJK* photometry are available. Preliminary results based on a sub-sample of the data discussed here were presented by Romaniello et al. (2005). Here we present the results about the iron content for the complete sample. In a forthcoming paper we will discuss the α-elements abundances.

The paper is organised as follows. The data sample is presented in Sect. 2. In Sect. 3 we thoroughly describe the data analysis and how we determine the metallicity of our stars. We compare our iron abundances with previous results in Sect. 4. The dependence of the PL relation on [Fe/H] is discussed in Sect. 5. Finally, Sect. 6 summarizes our concluding remarks.

2. The data sample

We have observed a total of 68 Galactic and Magellanic Cepheid stars. The spectra of the 32 Galactic stars were collected at the ESO 1.5 m telescope on Cerro La Silla with the Fibrefed Extended Range Optical Spectrograph (FEROS, Pritchard 2004). Two fibres simultaneously feed the spectrograph: one fibre records the object spectrum, while the second one is fed either by the sky background or by a calibration lamp to monitor the instrument stability during the exposure (the sky background was chosen in our case). The CCD is a thinned, back illuminated detector with 15 micron pixels (2048×4096 pixels). The resolving power is 48 000 and the accessible wavelength range is from 3700 to 9200 Å.

The spectra of the 22 Cepheids in the LMC and the 14 Cepheids in the SMC were obtained at the VLT-Kueyen telescope on Cerro Paranal with the UV-Visual Echelle Spectrograph (UVES, Dekker et al. 2000; Kaufer et al. 2004) in service mode. The detector in the Red Arm is a mosaic of two CCDs (EEV + MIT/LL) with 15 micron pixels (2048×4096 pixels). The resolving power is about 30 000 (corresponding to a slit of 100) and the spectral range covered in our spectra is from 4800 to 6800 Å (580 nm setting).

The 2D raw spectra were run through the respective instrument Data Reduction softwares, yielding 1D extracted,

Table 2. Pulsation phases (ϕ) and intrinsic parameters of the Galactic Cepheids. Both AP Pup and AX Vel were not included in the analysis of the metallicity effect because accurate distance estimates are not available in literature. In particular, for AP Pup we only listed the apparent mean magnitudes. In the last column is listed the duplicity status according to Szabados (2003): B – spectroscopic binary, Bc – spectroscopic binary that needs confirmation, O – spectroscopic binary with known orbit, V – visual binary.

ID	$\log P$	ϕ	$\mu_{\rm Old}$	$E(B-V)_{\rm Old}$	$\mu_{\rm New}$	$E(B-V)_{\rm New}$	M_B	M_V	M_K	Duplicity
l Car	1.5509	0.580	8.99^d	0.170^d	8.56^b	0.147^a	−4.17	−5.28	−7.53	. . .
U Car	1.5891	0.490	10.97^d	0.283^d	10.87^a	0.265^a	−4.50	−5.41	−7.44	B
V Car	0.8259	0.375	9.84^e	0.174^h	10.09^a	0.169^a	−2.54	−3.24	−4.86	B
WZ Car	1.3620	0.745	12.92^d	0.384^d	12.69^a	0.370^a	−3.80	−4.58	−6.52	. . .
V Cen	0.7399	0.155	9.18^d	0.289^c	8.91^a	0.292^a	−2.41	−2.99	−4.49	. . .
KN Cen	1.5319	0.867	13.12^d	0.926^d	12.84^a	0.797^a	−4.63	−5.46	−7.59	B
VW Cen	1.1771	0.967	12.80^d	0.448^d	12.76^a	0.428^a	−2.93	−3.85	−6.08	B
XX Cen	1.0395	0.338	11.11^d	0.260^d	10.90^a	0.266^a	−3.19	−3.91	−5.58	B
β Dor	0.9931	0.529	7.52^c	0.040^c	7.50^b	0.052^a	−3.16	−3.91	−5.57	. . .
ζ Gem	1.0065	0.460	7.78^c	0.010^c	7.81^b	0.014^a	−3.16	−3.94	−5.72	V
GH Lup	0.9675	0.031	10.05^e	0.364^h	10.25^a	0.335^a	−2.77	−3.66	−5.54	B
T Mon	1.4319	0.574	10.82^d	0.209^c	10.71^a	0.181^a	−4.16	−5.15	−7.25	O
S Mus	0.9850	0.266	9.81^e	0.147^h	9.57^a	0.212^a	−3.48	−4.10	−5.62	O
UU Mus	1.0658	0.865	12.59^d	0.413^d	12.41^a	0.399^a	−3.12	−3.86	−5.70	. . .
S Nor	0.9892	0.343	9.91^d	0.189^c	9.87^a	0.179^a	−3.23	−4.00	−5.77	B
U Nor	1.1019	0.422	10.72^d	0.892^d	10.46^a	0.862^a	−3.14	−3.90	−5.72	. . .
X Pup	1.4143	0.232	12.36^e	0.443^h	11.64^a	0.402^a	−3.57	−4.38	−6.34	. . .
AP Pup	0.7062	0.109	$. . .^f$	$. . .^f$	$. . .^f$	$. . .^f$	7.37	6.78	5.26	B
AQ Pup	1.4786	0.436	12.52^d	0.512^c	12.41^a	0.518^a	−4.53	−5.35	−7.27	B
BN Pup	1.1359	0.397	12.95^d	0.438^c	12.93^a	0.416^a	−3.55	−4.33	−6.14	. . .
LS Pup	1.1506	0.012	13.55^d	0.478^d	13.39^a	0.461^a	−3.60	−4.37	−6.18	B
RS Pup	1.6174	0.944	11.56^d	0.446^c	11.30^a	0.457^a	−4.71	−5.69	−7.81	. . .
VZ Pup	1.3649	0.816	13.08^d	0.471^c	12.84^a	0.459^a	−3.93	−4.63	−6.31	. . .
KQ Sco	1.4577	0.446	12.36^c	0.839^c	12.23^g	0.869^a	−4.05	−5.11	−7.55	. . .
EU Tau	0.3227	0.414	10.27^c	0.170^c	10.27^c	0.170^d	−2.26	−2.74	−4.05	Bc
SZ Tau	0.4981	0.744	8.73^c	0.290^c	8.55^a	0.295^a	−2.38	−2.93	−4.33	B
T Vel	0.6665	0.233	9.80^d	0.281^c	10.02^a	0.289^a	−2.24	−2.88	−4.47	B
AX Vel	0.5650	0.872	10.76^f	0.224^h	$. . .^f$	0.224^a	. . .	. . .	. . .	. . .
RY Vel	1.4496	0.704	12.02^d	0.562^c	11.73^a	0.547^a	−4.23	−5.05	−6.96	. . .
RZ Vel	1.3096	0.793	11.02^d	0.335^c	10.77^a	0.299^a	−3.78	−4.61	−6.56	. . .
SW Vel	1.3700	0.792	11.00^d	0.349^c	11.88^a	0.344^a	−4.02	−4.83	−6.75	. . .
SX Vel	0.9800	0.497	11.44^e	0.250^h	11.41^g	0.263^a	−3.33	−3.95	−5.49	. . .

^{a} Fouqué et al. (2007); ^{b} Benedict et al. (2007); ^{c} Groenewegen et al. (2004); ^{d} Storm et al. (2004); ^{e} Laney & Stobie (1995) and Groenewegen (2004); ^{f} not included in the analysis of the metallicity effect; ^{g} Groenewegen (2008); ^{h} Fernie et al. (1995).

wavelength calibrated and rectified spectra. The normalization of the continuum was refined with the IRAF task continuum. The 1D spectra were corrected for heliocentric velocity using the rvcorr and dopcor IRAF tasks. The latter was also used to apply the radial velocity correction, which was derived from 20 unblended narrow lines well spread over the spectrum, selected among the species Fe I, Fe II and Mg I. The measured signal-to-noise ratios vary between 70 and 100 for the FEROS spectra and between 50 and 70 for the UVES spectra.

The selected Cepheids span a wide period range, from 3 to 99 days. For the Galactic Cepheids we have adopted periods, optical and NIR photometry from Laney & Stobie (1994), Storm et al. (2004), Groenewegen et al. (2004), Benedict et al. (2007) and Fouqué et al. (2007). For the Magellanic Cepheids we have adopted periods, optical and NIR photometry from Laney & Stobie (1994). The pulsation phases at which our stars were observed and selected characteristics are listed in Tables 2 and 3 for the Galactic and the Magellanic Cloud Cepheids, respectively. Distance and reddening estimates for Galactic Cepheids come from two different samples. The "Old Sample" includes 32 Cepheids (see Cols. 4 and 5 in Table 2) and among them 25 objects have distance moduli provided by Storm et al. (2004,

see their Table 3) and by Groenewegen et al. (2004, see their Table 3). These distances are based on the infrared surface brightness method and the two different calibrations provide, within the errors, the same distances. For the remaining seven objects distance estimates are not available in the literature. For five of them we determined the distance by combining the linear diameter from Laney & Stobie (1995) with the V, K unreddened magnitudes from Laney & Stobie (1994), using two surface brightness-color calibrations:

– from Groenewegen (2004): we have combined Eqs. (1) and (2) with Table 3 coefficients marked with the filled circle (the V vs. $V − K$ relation);

– from Fouqué & Gieren (1997): we have combined Eq. (1) with Eq. (27) (the V vs. $V − K$ relation).

The distance moduli derived with the two calibrations mentioned above agree very well (within 1%) and we have adopted the distances determined with Groenewegen's calibration (these are the values listed in Table 2). The "New Sample" includes 32 Cepheids (see Cols. 6 and 7 in Table 2) and among them 24 objects have distance moduli based on the infrared surface brightness method provided by Fouqué et al. (2007, see

Table 3. Pulsation phases (ϕ) and intrinsic parameters of the Magellanic Cepheids. Periods ($\log P$), apparent mean magnitudes and reddenings come from Laney & Stobie (1994). The mean K-band magnitudes were transformed into the 2MASS photometric system using the transformation provided by Koen et al. (2007).

ID	$\log P$	ϕ	B_0	V_0	K_0	$E(B-V)$
			LMC			
HV 877	1.654	0.682	14.06	12.98	10.77	0.12
HV 879	1.566	0.256	14.12	13.15	11.03	0.06
HV 971	0.968	0.237	14.86	14.24	12.68	0.06
HV 997	1.119	0.130	14.94	14.19	12.37	0.10
HV 1013	1.382	0.710	14.39	13.46	11.41	0.11
HV 1023	1.425	0.144	14.48	13.51	11.45	0.07
HV 2260	1.112	0.144	15.19	14.43	12.67	0.13
HV 2294	1.563	0.605	13.19	12.45	10.74	0.07
HV 2337	0.837	0.861	...	...	13.27	0.07
HV 2352	1.134	0.201	14.49	13.84	12.25	0.10
HV 2369	1.684	0.136	13.15	12.29	10.38	0.10
HV 2405	0.840	0.037	...	...	13.43	0.07
HV 2580	1.228	0.119	14.33	13.67	11.92	0.09
HV 2733	0.941	0.411	14.85	14.34	13.00	0.11
HV 2793	1.283	0.917	14.49	13.58	11.75	0.10
HV 2827	1.897	0.880	13.19	12.03	9.80	0.08
HV 2836	1.244	0.059	14.85	14.02	12.04	0.18
HV 2864	1.041	0.055	15.16	14.42	12.77	0.07
HV 5497	1.997	0.321	12.73	11.63	9.43	0.10
HV 6093	0.680	0.024	15.74	15.16	13.71	0.06
HV 12452	0.941	0.860	15.25	14.60	12.83	0.06
HV 12700	0.911	0.342	15.62	14.87	13.12	–0.01
			SMC			
HV 817	1.277	0.298	14.13	13.59	12.12	0.08
HV 823	1.504	0.873	14.46	13.60	11.58	0.05
HV 824	1.818	0.315	13.06	12.27	10.33	0.03
HV 829	1.931	0.348	12.61	11.81	9.92	0.03
HV 834	1.866	0.557	12.95	12.14	10.20	0.02
HV 837	1.631	0.822	13.95	13.10	11.11	0.04
HV 847	1.433	0.500	14.40	13.66	11.83	0.08
HV 865	1.523	0.108	13.55	12.93	11.21	0.06
HV 1365	1.094	0.184	15.39	14.79	13.20	0.07
HV 1954	1.223	0.847	14.13	13.62	12.12	0.07
HV 2064	1.527	0.279	14.28	13.50	11.61	0.07
HV 2195	1.621	0.135	13.85	13.07	11.09	–0.02
HV 2209	1.355	0.822	13.99	13.42	11.84	0.04
HV 11211	1.330	0.516	14.36	13.64	11.83	0.06

their Table 7). The trigonometric parallaxes for l Car, β Dor, and ζ Gem have been provided by Benedict et al. (2007). For EU Tau, we adopted the distance by Groenewegen et al. (2004), while for KQ Sco and SX Vel we adopted distances calculated by one of us (MG), following the general method outlined in Groenewegen (2007), but using the SB-relation and projection-factor from Fouqué et al. (2007) for consistency. The Cepheid AP Pup was not included in the analysis of the metallicity effect because an accurate estimate of its linear diameter is not available. For this object in Table 2 we only listed the apparent magnitudes. The same outcome applies to AX Vel, since Laney & Stobie (1995) mentioned that the quality of the radius solution for this object was quite poor. Accurate reddening estimates for Galactic Cepheids have been recently provided by Laney & Stobie (2007), however, we typically adopted the reddening estimates used to determine individual Cepheid distances.

The current Cepheid sample includes objects that are classified in the literature as fundamental pulsators, except EU Tau and SZ Tau, which are classified as first overtone pulsators, and AX Vel that is classified as one of the few double-mode pulsators in the Galaxy (Fernie et al. 1995; Sziladi et al. 2007).

Indeed, when plotting our Cepheid sample in the $\log P$ vs. M_V plane, we confirm that EU Tau and SZ Tau are the only stars lying on the first overtone PL relation. Therefore, their observed periods have been "fundamentalised" using the relation $P_0 = P_1/(0.716 - 0.027 \log P_1)$ (Feast & Catchpole 1997).

Approximately, 50% of Galactic Cepheids in our sample are spectroscopic binaries (Szabados 2003) and one star (ζ Gem) is a visual binary (see last column of Table 2). According to current empirical evidence the companions are typically B and A-type main sequence stars, which are much less luminous (at least 3 mag) than our main Cepheid targets. Only in the case of the two most luminous B dwarf, companions respectively of KN Cen and S Mus, we have detected a small contribution to the continuum level of the Cepheid spectra. Its effect on the final iron abundances will be discussed in Sect. 4.
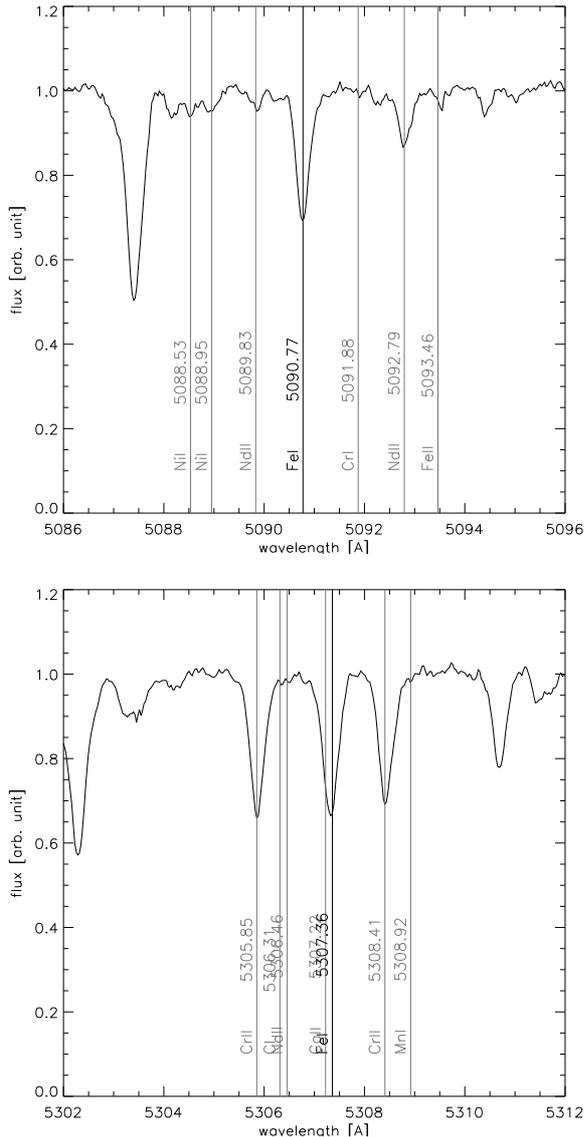
3. Methodology

Below we present the methodology used to assemble the linelist and to determine the equivalent widths and the atmospheric parameters of our programme stars. All of these are key ingredients in the calculation of elemental abundances.

3.1. Line list

A crucial step of any spectral analysis in order to derive elemental abundances is a careful assembling of a line list. We have assembled our Fe I–Fe II line list from Clementini et al. (1995), FC97, Kiss & Vinko (2000) and Andrievsky et al. (2002a) plus a selection of lines from VALD (Vienna Atomic Line Database; Kupka et al. 1999; Ryabchicova et al. 1999).The VALD lines have been selected for effective temperatures typical of Cepheid stars (4500–6500 K). We have, then, visually inspected each line on the observed spectra, in order to check their profile and to discard blended lines. In order to do so, we have searched the VALD database (with the command extract stellar) for all the existing lines between 4800 and 7900 Å on stellar spectra characterized by stellar parameters typical of Cepheids ($T_{\rm eff}$ = 4500 K, 5500 K and 6500 K, $\log g$ = 2 and $v_{\rm t}$ = 3 km s^{-1}). We have, then, over-plotted all the lines found in VALD, that fall within ±3 Å from each of our iron lines, and checked for their possible contribution to the equivalent width of our iron line (an example is shown in Fig. 2). This test was carried out on 3 different observed spectra, characterized by effective temperatures (as found in the literature from previous analyses) close to 4500 K, 5500 K and 6500 K, respectively. Any contribution larger than 5% of the line strength made us discard the iron line under scrutiny. There remains, of course, the possibility that some weak lines could be missing in the VALD compilation, but these are expected to be only weak lines, whose contribution would, then, be negligible.

Our final list includes 275 Fe I lines and 37 Fe II lines, spanning the spectral range covered by our FEROS spectra. Our UVES spectra cover a narrower spectral range for which we can use 217 Fe I lines and 30 Fe II lines. For all the lines, we have adopted the physical properties (oscillator strengths, excitation potentials) listed in VALD. Figure 3 shows the comparison between the distribution of the equivalent widths of our lines with those from FC97 for the Galactic Cepheid V Cen. As it can be clearly seen, our list is significantly larger and well samples the best range of equivalent widths, around 20 mÅ, as suggested by Cayrel (1988) to obtain reliable elemental abundances (iron in our case). The line list is presented in Table 4, where the four

Fig. 3. The distributions of the equivalent widths (EW) of our lines (empty histogram) and Fry & Carney's lines (1997, dark grey histogram), in the case of the same star (VCen).

Table 4. Iron line list, from left to right the columns display wavelength, ion identification, excitation potential (*EP*) and log *gf* values. The table is available in its entirety via the link to the machine-readable version. A portion is shown here for guidance regarding its form and content.

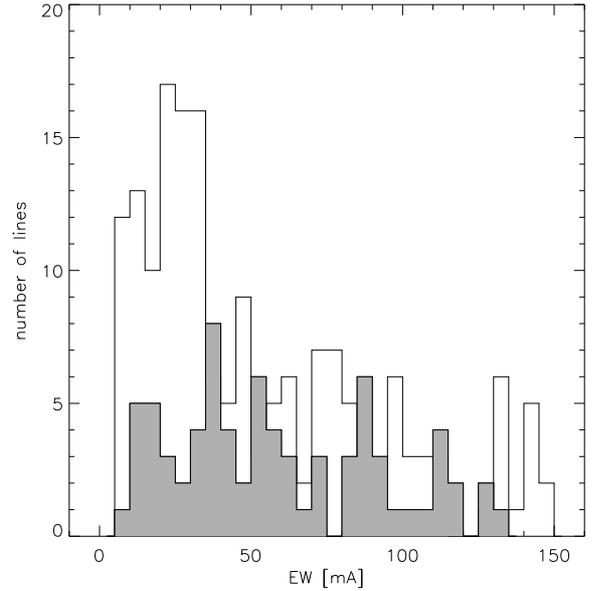| λ	Ion	*EP*	log *gf*
4892.87	Fe I	4.22	−1.34
4917.23	Fe I	4.19	−1.29
4924.77	Fe I	2.28	−2.24
4932.08	Fe I	4.65	−1.49
4950.10	Fe I	3.42	−1.67
4973.11	Fe I	3.96	−0.95
4994.13	Fe I	0.91	−3.08
5029.62	Fe I	3.41	−2.05
5044.21	Fe I	2.85	−2.04
5049.82	Fe I	2.28	−1.36
5054.64	Fe I	3.64	−1.92
5056.84	Fe I	4.26	−1.96
5067.15	Fe I	4.22	−0.97
5072.67	Fe I	4.22	−0.84
5083.34	Fe I	0.96	−2.96
. . .	. . .	. . .	. . .

Fig. 2. Examples of visual inspection on the selected iron lines. The iron lines are plotted in black while the other elemental lines are plotted in gray. *In the top panel* it is shown an unblended line, while *in the bottom panel* there is an example of a blended line.

columns list respectively the wavelength, the ion identification, the excitation potential and the g_f values of each line.

3.2. Equivalent widths

The second crucial step of our spectral analysis is the measurement of the equivalent widths (EW) of the iron lines we have assembled in our final list. At first, several independent and manual (i.e. with the IRAF splot task) measurements of the EW of the whole set of Fe I and Fe II lines in a selected number of Cepheids were performed in order to test the reproducibility of our measures. However, because of the large number of lines and spectra, our final EW measurements were derived by using a semi-interactive routine (fitline) developed by one of us (PF, *fitline*). This code is based on genetic algorithms, which mimic how DNA can be affected to make the evolution of species (Charbonneau 1995). It uses a Gaussian fit, which is defined by four parameters: central wavelength, width, depth and

continuum value of the line. A top-level view of the algorithm is as follows:

1. compute an initial set of Gaussians, picking random values of the four parameter (scaled to vary between 0 and 1) and calculate the χ^2 with the observed line for each Gaussian;
2. compute a new set of Gaussian from the 20 best fit of the previous "generation" introducing random modification in the values of the parameters ("mutation");
3. evaluate the "fitness" of the new set (χ^2 calculation for each Gaussian) and replace the old set with the new one;
4. iterate the process (100 to 200 "generations") to get the best fit (lowest χ^2) for each observed line.

All the UVES spectra have been smoothed to improve the quality of the Gaussian fit (smooth_step = 11 pix using *splot* task in IRAF). All the useful information from the spectra are preserved in the process. The selected iron lines, even on the

smoothed spectra, do not show any contamination from other line. However, for about 15% of the lines, the Gaussian profile performed by *fitline*, could not satisfactorily reproduce the observed profile. The equivalent widths of these lines, usually very broad or asymmetric, were measured manually with the *splot* task. The mean difference, as computed for those lines for which both methods could be applied, is around 1.5 mÅ, comparable to the average error on the EW inferred from the quality of the data (Eq. (7), Cayrel 1988). We can then safely use all our EW measurements, independently of the method we used to derive them.

For the determination of the metallicities, we have selected only lines with equivalent widths between 5 and 150 mÅ. The lower limit was chosen to be a fair compromise between the spectral characteristics and the need for weak lines for an optimal abundance determination. The upper limit was selected in order to avoid the saturated portion of the curve of growth. We note that a slightly higher upper limit (200 mÅ) was chosen for T Mon, SZ Tau and KQ Sco because these stars have very strong lines. This was done in order to keep the number of selected lines similar to the one used for the rest of the sample, after checking that this higher upper limit does not have any effect on the final metallicities derived for these three stars.

Considering the mean difference on the EW obtained with *fitline* and *splot* and the uncertainty in the continuum placement from two measurements of the EW (carried out independently by two of us) we assume ±3 mÅ as error on the equivalent widths for the lines below 100 mÅ and ±5 mÅ for the stronger features.

3.3. Stellar parameters

The stellar parameters were derived spectroscopically. We have determined the stellar effective temperature T_{eff} by using the line depth ratios method described in Kovtyukh & Gorlova (2000). It is based on weak neutral metal lines (in our case, less than 100 mÅ in equivalent width in order to exclude line broadening effects) with low excitation potentials, selected to obtain as close as possible pairs in wavelength space. Since the calibration of this method has been done using the FC97 scale of temperatures, our temperature scale is linked to theirs. The line depth ratios have the advantage of being independent of interstellar reddening and metallicity effects, uncertainties that instead plague other methods like the integrated flux method or colors calibrations (Gray 1994). The main uncertainties of the calibration of the line depth ratios, instead, lie in the accuracy of its zero point and slope, which have been thoroughly tested either with different colour-temperature relations or diameters measurements by Kovtyukh & Gorlova (2000). As a sanity check on our temperature determinations, we have analysed five individual spectra of Galactic Cepheid AP Puppis taken at different phases along the pulsation period (ϕ = 0.11 – observed twice –, 0.31, 0.51, 0.91). Four out of these five spectra have been collected in an independent observational campaign and the results have already been discussed by Lemasle et al. (2007). Figure 4 shows the effective temperatures derived for the five phases of AP Pup (filled squares) in comparison with the temperature variation estimated by Pel (1978) on the basis of accurate Walraven photometry. The agreement is indeed very good.

The total number of line depth ratios adopted to estimate the temperature ranges from 26 to 32 and from 20 to 28 for Galactic and Magellanic Cepheids, respectively. From this method, we have obtained effective temperatures with an intrinsic accuracy of about 40 K for the Galactic Cepheids and 50 K for the
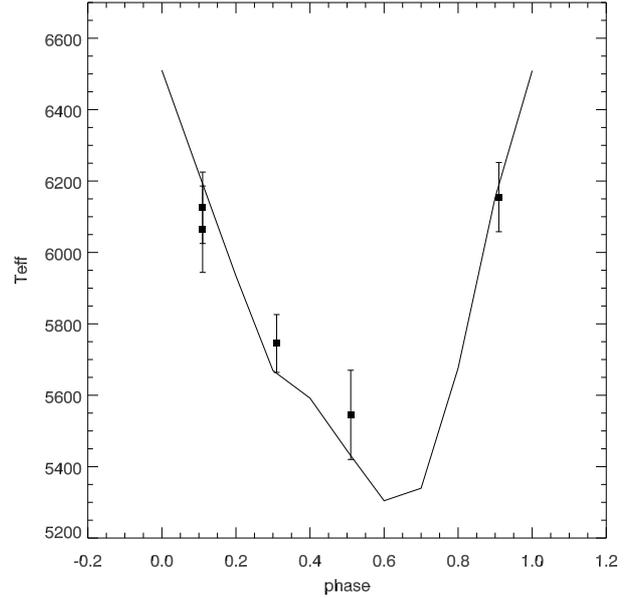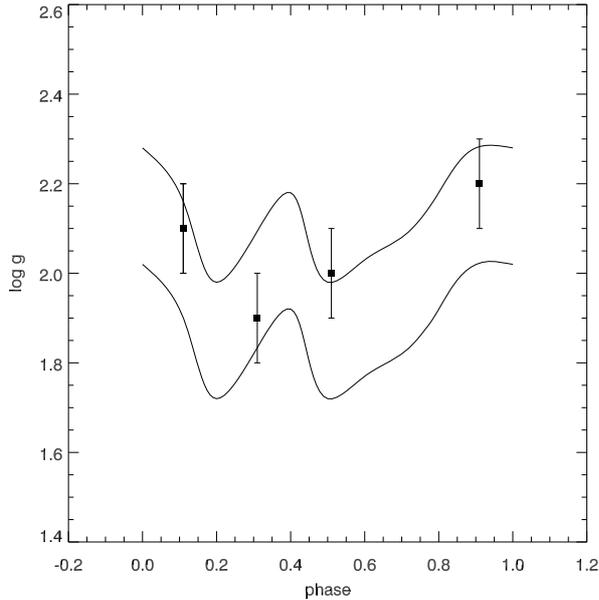

Fig. 4. Comparison between the behaviour of the effective temperature of the Galactic Cepheid AP Puppis found by Pel (1978, solid line) and our results using the line depth ratios method for 5 phases (filled squares) with their associate errorbars.

Magellanic ones (errors on the mean). Tables 7 and 9 list our final effective temperatures for Galactic and Magellanic Cepheids, respectively.

Microturbulent velocity (v_t) and gravity ($\log g$) were constrained by minimizing the log([Fe/H]) vs. EW slope (using the Fe I abundance) and by imposing the ionisation balance, respectively. These two procedures are connected and require an iterative process (on average, between 5 and 7 iterations, depending on the star). We first achieved the minimization of the log([Fe/H]) vs. EW slope and, subsequently, the ionisation balance. As first guess for the microturbulent velocity and the gravity, we adopted values typical of Cepheids (v_t = 3 km s^{-1}, $\log g$ = 2) as inferred from previous studies (FC97 and Andrievsky et al. 2002a,b).

We first assumed the ionisation balance to be fulfilled when the difference between [Fe I/H] and [Fe II/H] is less than the standard error on [Fe II/H] (typically, 0.08–0.1 dex). However, we noticed that for most stars this condition was usually satisfied by more than one value of $\log g$, suggesting that our conditions for fulfillment might be too conservative and not very informative. We then checked which $\log g$ value satisfies the ionisation balance within the standard error on [Fe I/H] (typically, 0.02 dex). For 55 stars out of 68 we were able to reach the Fe I–Fe II balance within few hundredths of a dex. The corresponding $\log g$ values are the final gravity values quoted in Tables 7 and 9. For the remaining 13 objects, we assumed as our final $\log g$ the value giving the "best" ionisation balance, i.e. the one with the smallest difference between [Fe I/H] and [Fe II/H]. Also, it is worth noticing that for two stars (HV 2827 and HV 11211) we had to increase the temperatures as determined from the line depth ratios by 50 K (which is still within the estimated error on the determination of T_{eff}), in order to fulfill our requirements for a satisfactory ionisation balance. Moreover, we note that the $\log g$ values derived for the five different phases of AP Puppis follow well the trend found by Pel (1978), as it can be seen in Fig. 5. At ϕ = 0.11, we have obtained the same value from the analysis of the two spectra.

Fig. 5. Comparison between the behaviour of the gravity of the Galactic Cepheid AP Puppis found by Pel (1978, the two solid lines indicate *the upper and lower limits*) and our results for 5 phases (filled squares) with their associate errorbars. At $\phi = 0.11$, we have obtained the same value from the analysis of the two spectra.
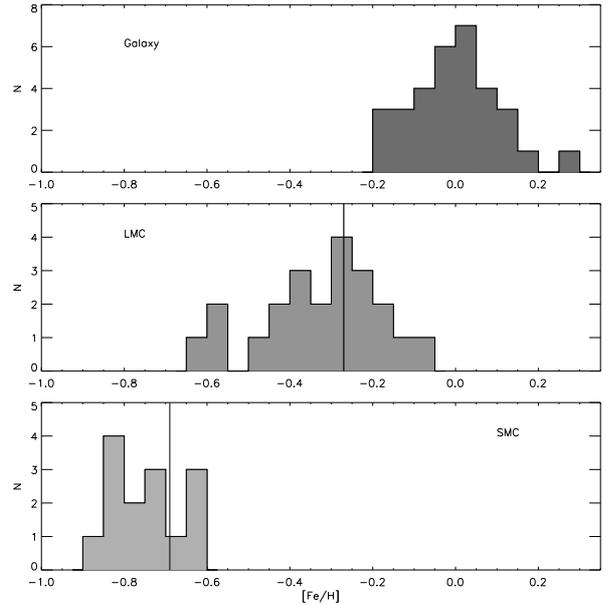

Fig. 6. Histograms of the [Fe/H] ratios derived for all the stars of our sample in the Galaxy, the LMC and the SMC. The solid lines indicate the mean values found using F and K supergiants by Hill et al. (1995) and Hill (1997) (see Table 8 and Sect. 4.3). We found a good agreement with the results obtained for non-pulsating stars of the same age of Cepheids.

In order to determine the errors on the microtutbulent velocity and the gravity, we have run several iterations for each star, slightly modifying the values of these two quantities that fulfill the requirements mentioned above. We have estimated errors in v_t to be 0.1 km s^{-1} and in $\log g$ to be 0.10 dex.

3.4. Model atmospheres

We have derived the iron abundances of our stars by using the Kurucz WIDTH9 code (Kurucz 1993) and LTE model atmospheres with the new opacity distribution functions (ODFs) computed by Castelli & Kurucz (2003). These models neglect envelope overshooting. We have used a grid of solar metallicity models for the Galactic and LMC Cepheids and a grid of models computed assuming [Fe/H] = −1.0 and an α-element enhancement of +0.4 dex for the SMC Cepheids (Gratton et al. 2004). The grids of models have been interpolated in temperature in order to match the effective temperature derived for each star with the line depth ratio method and in 0.10 dex gravity steps.

Our choices of model atmospheres (in terms of ODFs, overshooting, metallicity, and α-enhancement) have been thoroughly tested. A comparison between model atmospheres computed with the new ODFs (Castelli & Kurucz 2003, hereafter identified as the 2003 models) and the old ODFs (Castelli et al. 1997, hereafter identified as the 1997 models) shows small differences in the derived iron abundances: ∼0.01−0.03 dex. We tested the effect of different treatments of overshooting as implemented in different versions of Kurucz models by running the WIDTH9 code with two sets of the 1997 models computed with and without the "approximate" overshooting. Differences in the final iron abundances amount to 0.05 dex for Galactic and SMC Cepheids and around 0.06 dex for LMC Cepheids, with the models without overshooting giving the lower abundances.

Since the LMC has a mean metallicity around −0.3 dex, for this galaxy we also tested model atmospheres computed for [Fe/H] = −0.5 dex, finding differences of the order

of ∼0.01−0.02 dex in the derived iron abundances compared to the solar metallicity models. Similar differences are found when the [Fe/H] = −0.5 dex models are used also for the Small Magellanic Cloud (its mean metallicity is around −0.7/−0.8 dex). No differences in the derived iron content have been found between models computed with and without the +0.4 dex α-enhancement.

In all our computations, we have adopted a solar iron abundance of $\log[n(\mathrm{Fe})] = 7.51$ on a scale where $\log[n(\mathrm{H})] = 12$ (Grevesse & Sauval 1998) and we have assumed our final stellar metallicity to be the Fe I value, which has been derived by a far larger number of lines with respect to Fe II.

4. Iron abundances

Our final iron abundances, together with the adopted stellar parameters, are listed in Tables 7 and 9 for the Galactic and Magellanic Cepheids, respectively.

For our Galactic sample, we find that the mean value of the iron content is solar ($\phi = 0.10$, see Fig. 6), with a range of values between −0.18 dex and +0.25 dex. These two extremes are represented respectively by 2 and 1 stars (out of the 32 in total). Our Galactic Cepheids span a narrow range of Galactocentric distances (the mean Galactocentric distance of our sample is 7.83 ± 0.88 kpc, see Fig. 7), thus preventing us from giving any indications about the metallicity gradient in the Galactic disc.

For the LMC sample, we find a mean metallicity value of ∼−0.33 dex ($\phi = 0.13$, see Fig. 6), with a range of values between −0.62 dex and −0.10 dex. Here, the more metal-rich extreme is just an isolated case, while the metal-poor end of the distribution is represented by 3 stars.

For the SMC sample, we find that the mean value is about ∼−0.75 dex ($\phi = 0.08$, see Fig. 6), with a range of values between −0.87 and −0.63.
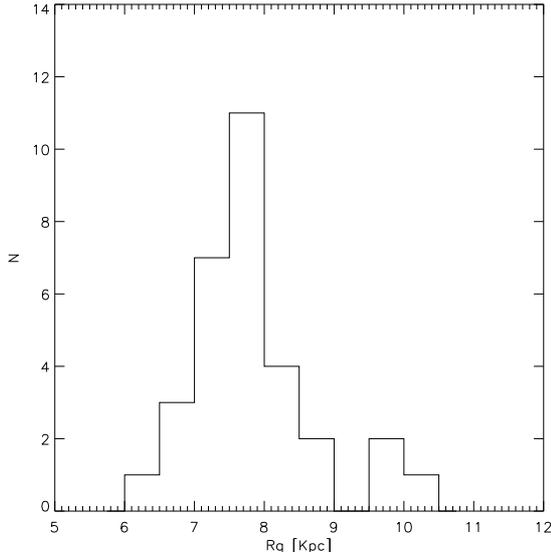
Fig. 7. Histograms of the Galactocentric distances derived for all the Galactic Cepheids with individual heliocentric distances.

As we have already mentioned in Sect. 2, there are two binary stars (KN Cen and S Mus) among our Galactic sample with a bright B dwarf as a companion. In the spectral range covered by our spectra, these bright companions give a contribution only to the continuum level, because all their absorption lines fall in the ultra-violet region (these are very hot stars, with effective temperature ~20 000 K). In order to test the effect of this contribution, we have subtracted from the observed spectrum of the two binaries the estimated optical spectrum of the B dwarf, which only consists of a continuum without any line. On the resulting spectra, which we assume to be the true spectra of our Cepheids, we have then remeasured the EWs of a sub-set of iron lines and derived the metallicity. In the case of KN Cen the differences in the EWs measured on the observed spectrum and the true Cepheid spectrum are negligible (i.e. within the errors), thus the iron content we have derived for this star is robust. Regarding S Mus, instead, the EWs measured on the true spectrum are 12−15% larger than the ones measured on the spectrum we have observed. Thus, the true iron abundance of this Cepheid star should be 0.1 dex higher than the one we have derived. This happens because the intensity of the lines (due only to the Cepheid contribution) when compared to the continuum of the combined spectra is, in percentage, less than the intensity of the lines compared to the continuum of the Cepheid alone. In other words the contribution of the companion makes the lines of the Cepheid weaker. Please note that the iron content reported for S Mus in Table 7 has already been corrected for the above mentioned effect.

4.1. Uncertainties

The internal uncertainties in the resulting abundances are due to errors in the atomic data (gf-values) and EW measurements. We have estimated, on average, an internal error in the [Fe/H] determination of 0.10 dex.

It is also important to understand the effects of potential systematic errors in the stellar parameters on the final derived abundances (see Table 5). In order to do so we have determined curves of growth for different effective temperatures, microturbulent velocities and gravities for both Fe I and Fe II. As

Table 5. Effects on measured Fe I and Fe II abundances caused by changes in atmospheric parameters.

	Δ[Fe I/H]	Δ[Fe II/H]
ΔT_{eff} = +100 K	+0.07 dex	+0.00 dex
$\Delta \log g$ = +0.1 dex	+0.00 dex	+0.04 dex
Δv_t = +0.1 km s^{-1}	–0.03 dex	–0.02 dex

Table 6. Stellar parameters and iron abundances along the pulsation cycle of the Galactic Cepheid AP Puppis. Phase 0.11 was observed twice 50 days apart, leading to very consistent results.

Phase	T_{eff}	v_t	$\log(g)$	[Fe/H]
0.11	6070	3.05	2.1	–0.07
0.11	6130	3.00	2.1	–0.03
0.31	5750	2.80	1.9	–0.03
0.51	5550	3.30	2.0	–0.06
0.91	6160	4.20	2.2	–0.13

expected, we find that Fe I abundances marginally depend on the gravity, whereas Fe II does not depend on the effective temperature. An increase in temperature of 100 K, at fixed v_t and $\log g$, results in an increase in [Fe I/H] of about 0.07 dex. An increase in v_t of 0.1 km s^{-1} gives a decrease in [Fe I/H] of about 0.03 dex, for constant T_{eff} and $\log g$, and we obtain a decrease of 0.02 dex for [Fe II/H]. An increase in $\log g$ of about 0.1 dex produces an increase in [Fe II/H] of about 0.04 dex (with fixed v_t and T_{eff}).

An additional potential source of uncertainty and concern comes from the fact that our metallicities have been derived from single epoch observations. However, we note that FC97 did not find any significant difference in their derived [Fe/H] as a function of phase (the test was performed on four of their longest period cepheids) and Luck & Andrievsky (2004) and Kovtyukh et al. (2005) show that the elemental abundances for Cepheids with a period between 6 and 68 days are consistent for all pulsation phases. Moreover, our exercise on AP Puppis (see Sect. 3.3 and Table 6) further confirms these conclusions, for a star even with a shorter period (5 days). As it can be seen in Table 6, not only do the derived stellar parameters nicely follow the expectations from photometry, as shown in Figs. 4 and 5, but the metallicities measured at all phases agree within the errors (~0.1 dex).

4.2. Comparison with previous studies on Cepheids

Before we address the key issue concerning the metallicity dependence of the Cepheid PL relation (cf. Sect. 5), let us first compare our results to previous works. For this purpose, we have selected the chemical analyses of FC97, Andrievsky et al. (2002a,b,c) and Luck et al. (2003) for the Galactic Cepheids and LL92 and L98 for the Magellanic Clouds. When necessary, we have rescaled the literature [Fe/H] values to the solar iron abundance we have adopted ($\log[n(\text{Fe})]$ = 7.51). One should keep in mind that the same stars have likely been observed at different phases and analysed with different tools and model atmospheres, which may lead to the determination of different combinations of stellar parameters. In the case of observations at different phases, as we already mentioned in the previous section, our results on the five spectra of AP Pup and the conclusions of Luck & Andrievsky (2004) and Kovtyukh et al. (2005) show that the elemental abundances do not depend on the phase. When multi-phase observations of the same star were available in the literature (this is the case for some of the Galactic Cepheids), we have compared the [Fe/H] values obtained for the same phase

Table 7. Stellar parameters and Fe I and Fe II abundances of our Galactic sample. The Fe I values have been adopted as final [Fe/H]. We compare our results, where it is possible, with previous investigations: Fry & Carney (1997); Andrievsky et al. (2002a,b,c); Luck et al. (2003).

ID	T_{eff}	v_t	$\log g$	[Fe I/H]	[Fe II/H]	[Fe/H]$_{FC}$	[Fe/H]$_A$
l Car	4750	3.60	0.4	0.00	0.00	. . .	. . .
U Car	5980	3.00	1.2	+0.17	+0.13	. . .	. . .
V Car	5560	3.05	1.8	–0.07	–0.02	. . .	. . .
WZ Car	4520	1.80	2.1	+0.08	+0.19	. . .	. . .
V Cen	6130	2.80	1.9	+0.04	–0.03	–0.12	+0.04[a]
KN Cen	5990	3.80	1.6	+0.17	+0.09	. . .	. . .
VW Cen	5240	4.20	1.2	–0.02	+0.07	. . .	. . .
XX Cen	5260	2.95	1.3	+0.04	+0.04	. . .	. . .
β Dor	5180	3.00	1.3	–0.14	–0.11	. . .	–0.01[a]
ζ Gem	5180	3.70	1.4	–0.19	–0.14	–0.04	+0.06[a]
GH Lup	5480	3.60	1.5	+0.05	+0.01	. . .	. . .
T Mon	4760	3.80	0.6	–0.04	–0.03	+0.09	+0.21[b]
S Mus	5780	2.75	1.8	+0.13	+0.19	. . .	. . .
UU Mus	5900	3.05	1.7	+0.11	+0.05	. . .	. . .
S Nor	5280	2.80	1.1	+0.02	+0.04	–0.05	+0.06[a]
U Nor	5230	2.60	1.1	+0.07	+0.13	. . .	. . .
X Pup	5850	3.30	1.4	+0.04	–0.05	. . .	0.00[a]
AP Pup	6070	3.05	2.1	–0.07	–0.07	. . .	. . .
AQ Pup	5170	3.10	0.8	–0.07	–0.09	. . .	–0.14[b]
BN Pup	5050	2.95	0.6	–0.10	–0.07	. . .	+0.01[c]
LS Pup	6550	3.50	2.2	–0.16	–0.10	. . .	. . .
RS Pup	4960	3.50	0.7	+0.09	+0.10	. . .	+0.16[b]
VZ Pup	5230	3.25	1.1	–0.17	–0.15	. . .	–0.16[c]
KQ Sco	4840	3.60	0.7	+0.21	+0.27	. . .	+0.16[d]
EU Tau	6060	2.30	2.1	+0.04	+0.02	. . .	–0.03[a]
SZ Tau	5880	2.80	1.7	+0.07	+0.04	–0.02	+0.06[a]
T Vel	5830	2.55	1.8	+0.10	+0.03	. . .	–0.04[b]
AX Vel	5860	3.10	1.8	+0.02	–0.06	. . .	. . .
RY Vel	5250	4.10	1.2	–0.07	–0.06	. . .	–0.03[b]
RZ Vel	5140	4.40	1.6	–0.19	–0.14	. . .	–0.11[b]
SW Vel	6590	3.75	1.7	–0.24	–0.17	–0.10	–0.05[b]
SX Vel	5380	2.55	1.2	+0.02	–0.02	. . .	–0.04[b]

[a] Luck et al. (2003); [b] Andrievsky et al. (2002a); [c] Andrievsky et al. (2002c); [d] Andrievsky et al. (2002b).

of our observations. Otherwise, we chose the iron content corresponding to the closest value of effective temperature to ours. Regarding the determination of different sets of stellar parameters, we do not have the capabilities (in terms of analytical codes and different sets of model atmospheres) in order to properly take this into account. However, we did signal such differences whenever we noted them.

In total, for the Galactic sample, we have 6 stars in common with FC97 and 18 with the entire sample of Andrievsky's group, while for the MC sample, we have 3 stars in common with LL92 and 7 with L98.

4.2.1. Galactic Cepheids

The mean difference between our results and those of FC97 and Andrievsky analyses is comparable to the difference between FC97 and Andrievsky's values (0.08 ± 0.02). In more detail, the mean difference between our iron abundances and FC97 is 0.09 ± 0.02, which is satisfactory. For 4 stars (V Cen, S Nor, TMon, ζ Gem) the agreement is at 1σ level, for the remaining 2 stars (we have 6 in common, in total) the agreement is well within the quoted uncertainties. We note that our derived abundances for V Cen and S Nor are more in agreement with the metallicity derived by Andrievsky et al. than with FC97.

When comparing our results to Andrievsky's, we obtain a mean difference of 0.07 ± 0.05. For 14 stars (out of 18), the

Table 8. Comparison of the mean metallicities of the Magellanic Clouds with previous studies. The number of studied stars are also listed. RB89: Russell & Bessell (1989); RD92: Russell & Dopita (1992); R93: Rolleston et al. (1993); H95: Hill et al. (1995); H97: Hill (1997); K00: Korn et al. (2000); A01: Andrievsky et al. (2001); R02: Rolleston et al. (2002); G06: Grocholski et al. (2006); T07: Trundle et al. (2007); P08: Pompeia et al. (2008).

Reference	[Fe/H]$_{LMC}$	[Fe/H]$_{SMC}$	Notes
This work	–0.33 ± 0.13	–0.75 ± 0.08	22 + 14 Cepheids
RB89	–0.30 ± 0.20	–0.65 ± 0.20	8 + 8 F supergiants
R93	. . .	–0.80 ± 0.20[a]	4 B stars
H95	–0.27 ± 0.15	. . .	9 F supergiants
H97	. . .	–0.69 ± 0.10	6 + 3 K supergiants
K00	–0.40 ± 0.20	–0.70 ± 0.20	6 B stars
A01	–0.40 ± 0.15	. . .	9 F supergiants
R02	–0.31 ± 0.04	. . .	5 B stars
G06	–0.3 – –2.0[b]	. . .	200 giants
T07	–0.29 ± 0.08	–0.62 ± 0.14	13 + 5 cluster giants
P08	–0.3 – –1.8	. . .	59 red giants

[a] Mean metallicity based on oxygen. [b] Metallicity based on calcium triplet.

iron abundances agree quite well within the associated errors. Of the remaining 4 stars, we note that SW Vel, β Dor, and T Mon agree within the standard deviation (σ = 0.20, 0.19, 0.22 dex respectively) instead of the standard error, that is the condition

Table 9. Stellar parameters and Fe I, Fe II abundances of our Magellanic Cepheids. The Fe I values were adopted as final [Fe/H]. When available the value from previous studies is also reported ([Fe/H]$_L$, where L stands for Luck & Lambert 1992; Luck et al. 1998). In the last column are listed the same values (as in Col. #7), but rescaled to the iron solar abundance adopted in our work.

ID	T_{eff}	v_t	$\log g$	[Fe I/H]	[Fe II/H]	[Fe/H]$_L$	[Fe/H]$_{LC}$
			LMC				
HV 877	4690	5.40	0.5	–0.44	–0.47	. . .	. . .
HV 879	5630	3.05	1.0	–0.14	–0.14	–0.56[b]	–0.46
HV 971	5930	2.30	1.4	–0.29	–0.29	. . .	. . .
HV 997	5760	3.10	1.2	–0.21	–0.22	. . .	. . .
HV 1013	4740	5.35	0.2	–0.59	–0.60	. . .	. . .
HV 1023	5830	3.10	1.1	–0.28	–0.27	. . .	. . .
HV 2260	5770	3.40	1.6	–0.38	–0.36	. . .	. . .
HV 2294	5080	3.90	0.5	–0.42	–0.42	–0.06[a]	+0.10
HV 2337	5560	3.30	1.6	–0.35	–0.36	. . .	. . .
HV 2352	6100	3.65	1.6	–0.49	–0.47	. . .	. . .
HV 2369	4750	6.00	0.3	–0.62	–0.63	. . .	. . .
HV 2405	6170	4.20	2.3	–0.27	–0.28	. . .	. . .
HV 2580	5360	2.75	0.7	–0.24	–0.25	. . .	. . .
HV 2733	5470	2.90	1.8	–0.28	–0.27	. . .	. . .
HV 2793	5430	2.90	0.9	–0.10	–0.11	. . .	. . .
HV 2827	4790	4.00	0.0	–0.38	–0.33	–0.24[b]	–0.14
HV 2836	5450	2.85	1.0	–0.16	–0.19	. . .	. . .
HV 2864	5830	2.80	1.5	–0.19	–0.20	. . .	. . .
HV 5497	5100	3.40	0.3	–0.25	–0.24	–0.48[b]	–0.38
HV 6093	5790	4.50	1.5	–0.60	–0.60	. . .	. . .
HV 12452	5460	2.90	1.0	–0.35	–0.37	. . .	. . .
HV 12700	5420	3.15	1.4	–0.36	–0.35	. . .	. . .
			SMC				
HV 817	5850	3.25	1.0	–0.82	–0.84	. . .	. . .
HV 823	5990	3.80	1.4	–0.80	–0.81	. . .	. . .
HV 824	5170	3.00	0.7	–0.73	–0.74	–0.94[b]	–0.84
HV 829	5060	3.30	0.2	–0.76	–0.73	–0.61[b]	–0.51
HV 834	5750	2.95	1.2	–0.63	–0.64	–0.59[b]	–0.49
HV 837	5140	2.90	0.0	–0.83	–0.80	–0.91[b]	–0.81
HV 847	4790	2.80	0.0	–0.75	–0.77	. . .	. . .
HV 865	6130	1.90	0.5	–0.87	–0.82	–0.44[a]	–0.28
HV 1365	5340	2.48	0.6	–0.82	–0.84	. . .	. . .
HV 1954	5890	2.47	1.0	–0.76	–0.75	. . .	. . .
HV 2064	5550	3.10	0.7	–0.64	–0.64	. . .	. . .
HV 2195	5970	2.90	1.0	–0.67	–0.68	–0.45[a]	–0.29
HV 2209	6130	2.30	1.1	–0.65	–0.67	. . .	. . .
HV 11211	4830	2.60	0.0	–0.83	–0.81	. . .	. . .

[a] Luck & Lambert (1992); [b] Luck et al. (1998).

suggested by Kovtyukh et al. (2005a) for the independence of the elemental abundance on the phase. This is not the case for ζ Gem, for which we cannot explain the difference (0.20 dex) but for which we find instead an agreement with FC97.

4.2.2. Magellanic Cepheids

In order to properly compare our results for the Magellanic Cepheids with the values obtained by LL92 and L98, we first had to rescale the latter values for the difference in the adopted solar iron abundance between us (7.51) and them (7.67 and 7.61, respectively). These revised values are listed in the last column of Table 9.

In general, the mean metallicities that L98 found with their complete sample (−0.30 dex and −0.74 dex for the LMC and SMC, respectively) are in very good agreement with our results (−0.33 dex and −0.75 dex). They also found a similar spread in iron for the MCs. With LL92, instead, there is a good agreement in the case of LMC but a difference for the metallicity of the SMC (0.15 dex greater than our mean value). Our derived abundances are always smaller than the values derived by LL92.

However, the number of objects in common is too small to constrain the effect on a quantitative basis.

When we move to a star-by-star comparison, larger differences emerge. The comparison with L98 abundances discloses a very good agreement for one object (HV 837) and a plausible agreement, i.e. within the standard deviation error, for other 3 stars (HV 5497, HV 824 and HV 834). Regrettably, this is not the case of HV 879, HV 2827 and HV 829 for which we note rather large discrepancies (∼0.2−0.3 dex) that remain unexplained. However, we note that L98 used different analytical codes, different oscillator strengths, and different values of the stellar gravity (they adopted the "physical" gravity calculated from the stellar mass, the luminosity and the temperature). A combination of all these three factors could well account for the observed differences.

As already mentioned, larger differences (0.4−0.6 dex) are found with respect to LL92, for the 3 stars we have in common. Following the referee suggestion we performed a more quantitative comparison for the three Cepheids in common with LL92, namely HV 865, HV 2195 and HV 2294. The calibrated spectra were kindly provided in electronic form by Luck. By

adopting the same atmospheric parameters used by LL92 we find the following iron abundances: [Fe I/H] = −0.75 (HV 865), −0.60 (HV 2195) and −0.15 (HV 2294). The comparison with the iron abundances provided by LL92 (see the last column in Table 9) indicates that the new measurements are ∼0.3 dex systematically more metal-poor. They also agree, within the errors, reasonably well with current measurements (see Col. 5 in Table 9). Thus supporting the arguments quoted above to account for the difference between the two different iron measurements. Moreover, one should keep in mind that the quality of the LL92 data set is significantly lower than ours ($R \approx$ 18 000 vs. 40 000) and that their oscillator strengths may differ from our selection: they were taken from the critical compilations of Martin et al. (1988) and Fuhr et al. (1988), which are included in VALD but not among the references used for our gf-values. Moreover, they have used different analytical tools: MARCS model atmospheres (Gustafsson et al. 1975) and a modified version of the LINES line-analysis code and MOOG (Sneden 1973) synthesis code. They also state that their method overestimates the equivalent widths of the weak lines.

4.3. A comparison with different stellar populations in the Magellanic Clouds

The mean metallicities of our Magellanic sample are in good agreement with previous results obtained for F, K supergiants and B stars in the Magellanic Clouds (see Table 8).

Russell & Bessell (1989) found a mean [Fe/H] = −0.30 ± 0.2 dex in the LMC and [Fe/H] = −0.65 ± 0.2 dex in the SMC, analysing high-resolution spectra of 16 F supergiants (8 for each galaxy). In 1995 Hill et al. obtained, from 9 F supergiants from the field of the LMC, a mean iron abundance of −0.27 ± 0.15 dex and Hill (1997) found a mean [Fe/H] = −0.69 ± 0.1 dex, analysing 6 K supergiants in the SMC. Andrievsky et al. (2001) re-analysed the sample of F LMC supergiants studied by Hill et al. (1995) and obtained a slightly lower mean value: [Fe/H] = −0.40 ± 0.15 dex.

Regarding the B type stars, Rolleston et al. (1993) and Rolleston et al. (2002) found, from the analysis of 4 stars in the SMC and 5 stars in the LMC, respectively, mean values of metallicity of −0.8 ± 0.20 dex and −0.31 ± 0.04 dex. Korn et al. (2000) obtained for the LMC (from 6 B stars) a mean [Fe/H] = −0.40 ± 0.2 dex and [Fe/H] = −0.70 ± 0.2 dex for the SMC (from 3 B stars). Grocholski et al. (2006) using homogeneous calcium triplet measurements for 200 stars belonging to 28 different LMC clusters covering a broad range of cluster ages, found by transforming the Ca abundance in iron abundance that the metallicity ranges from [Fe/H] ∼ −0.3 to [Fe/H] ∼ −2.0. More recently, Trundle et al. (2007) collected high resolution spectra with FLAMES@VLT for a good sample of Magellanic giants and found a mean metallicity of [Fe/H] = −0.62 ± 0.14, 5 giants in the SMC cluster NGC 330, and of [Fe/H] = −0.29 ± 0.08, 13 giants in the LMC cluster NGC 2004. By using similar data for 59 red giant stars in the LMC inner disk, Pompeia et al. (2008) found that their metallicity ranges from [Fe/H] ∼ 0.0 to [Fe/H] ∼ −1.80.

In conclusion, the mean iron content of Cepheids, for the Magellanic Clouds, agree very well with the results obtained for non variable stars of similar age and stars that are Cepheid's progenitors. Cepheids do not show any difference with these two other populations.

5. The effect of [Fe/H] on the PL relation

To assess the effect of the iron content on the Cepheid PL relation we select, among our sample, only the stars with periods between 3 and 70 days (61 stars out of 68), populating, in this way, the linear part of the PL relation, i.e. the one useful for distance determinations (e.g. Bono et al. 1999; Marconi et al. 2005).

By using the values given in the current literature (e.g. Benedict et al. 2002; Walker 2003; Borissova et al. 2004; Sollima et al. 2008; Catelan & Cortes 2008; Groenewegen et al. 2008), we adopted for the barycentre of the LMC a true distance modulus (μ_{LMC}) of 18.50 mag (with an error of ±0.10). This is also consistent with the standard PL relations (Freedman et al. 2001; Persson et al. 2004) used as comparison. The SMC is considered 0.44 ± 0.10 mag more distant than the LMC (e.g. Cioni et al. 2000; Bono et al. 2008). This value of the relative distance between the two galaxies has confirmed the results of previous studies (Westerlund 1997, and references therein). For all the Galactic Cepheids we have individual distances, as mentioned in Sect. 2 above.

It is necessary to divide our Cepheid sample into bins of metallicity to investigate its effect on the PL relation. The number of bins needs to be chosen taking into account two competing effects. On the one hand, dividing the stars in more bins in principle allows to disentangle finer details. On the other, however, each bin needs to contain enough stars so that the instability strip is well populated and, hence, spurious sampling effects are negligible. We choose two bins with about 30 stars each as best compromise between a detailed investigation and statistical significance. This choice is justified by the simulations described in the next section.

Our results for the V and K bands are presented in Figs. 8 and 9, respectively. In the top panels are shown the PL relations in each metallicity bin calculated with a linear regression. In each panel are also indicated the average iron content of the bin, the root mean square of the linear regression and the number of stars.

The bottom panels of Figs. 8 and 9 show the magnitude residuals $\delta(M)$ in the V and K band, respectively, as a function of [Fe/H]. These magnitude residuals are calculated as the difference between the observed absolute magnitude and the absolute magnitude as determined from its period using a standard PL relation, namely the PL_V from Freedman et al. (2001) and the the PL_K band Persson et al. (2004). In practice, $\delta(M)$ is the correction to be applied to a universal, [Fe/H]-independent PL relation to take into account the effects of metallicity. A positive δ means that the actual luminosity of a Cepheid is fainter than the one obtained with the standard PL relation. The filled squares in the bottom panels of Figs. 8 and 9 represent the mean values of $\delta(M)$ in each metallicity bin, the vertical error-bars are the errors on the mean and the solid line is the null value, which corresponds to an independence of the PL relation on the iron content. The horizontal bars indicate the size of the metallicity bins.

Data plotted in the bottom right panel of Fig. 8 indicate that the magnitude residuals of the V band in the individual bins are positive and located at ≈2σ (metal-poor) and ≈9σ (metal-rich) from zero. Moreover, the $\delta(M_V)$ in the two bins differ from each other at the 3σ level. Our data, then, suggest that metal-rich Cepheids in the V band are, at a fixed period, fainter than metal-poor ones. Data plotted in the bottom left panel indicate that this finding is marginally affected by uncertainties in the Galactic Cepheid distance scale. The use of Cepheid distances provided by Groenewegen (2008) provides a very similar trend
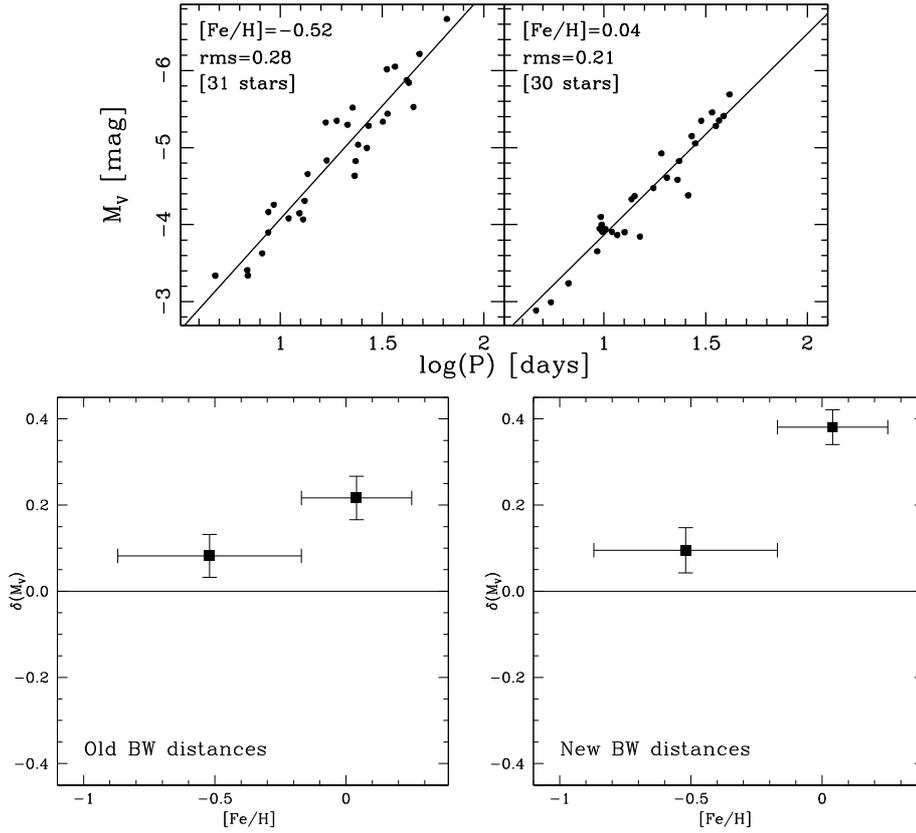
Fig. 8. *The top panels* show the PL relations calculated in each bin for the *V* band. *The bottom panels* show the residuals $\delta(M_V)$ as a function of the iron abundance for both the "Old" and the "New" Galactic Cepheid distances. The mean values of $\delta(M_V)$ in each metallicity bin are plotted as filled squares, with the vertical error-bars representing its associated error. The horizontal bars indicate the dimension of the bins. The horizontal solid lines indicate the null value which corresponds to an independence of the PL relation from the iron content.

concerning the metallicity effect. Moreover, the magnitude residuals based on the "Old Sample" are located $\approx1.5\sigma$ (metal-poor) and $\approx4\sigma$ (metal-rich) from zero and the difference in the two bins is larger than one σ.

The results for the *K* band are displayed in Fig. 9. The near-infrared data are on different photometric systems, therefore, we transformed them into the 2MASS (Two Micron All Sky Survey) photometric system. In particular, the apparent *K* magnitudes listed in Tables 2 and 3 were transformed using the transformations provided by Koen et al. (2007), while the PL$_K$ relation by Persson was transformed using the transformations provided by Carpenter (2001). The correction are typically of the order of ~0.02 mag. Data plotted in the bottom right panel of Fig. 9 indicate that the metal-poor bin is within 1σ consistent with zero. On the other hand, the metal-rich bin differs from the null hypothesis by $\approx4\sigma$. Moreover, the magnitude residuals in the two metallicity bins differ by $\approx2\sigma$. This finding is at odds with current empirical (Persson et al. 2004; Fouqué et al. 2007) and theoretical (Bono et al. 1999, 2008; Marconi et al. 2005) evidence suggesting that the PL$_K$ relation is marginally affected by metal abundance. In order to constrain this effect we also adopted the "Old Sample" distances. The magnitude residuals plotted in the bottom right panel of Fig. 9 show that the two metallicity bins are, within the errors, consistent with no metallicity effect. Unfortunately, current error budget (distance, metal abundance) does not allow us to reach firm conclusions concerning the metallicity dependence of the PL$_K$ relation.

### 5.1. Estimation of the errors caused by sampling of the PL

The error on the residuals showed in Figs. 8 and 9 is characteristic of the particular sample of stars we have used. In this section

we describe the simulations we have performed in order to assess the impact of different samplings of the PL relation.

In order to do so, we have extracted random subsamples composed by different numbers of stars from a sample of observed Cepheid that populate well the PL relation. We choose as reference a sample of 771 LMC Cepheids from the OGLE database (Udalski et al. 1999) for the test in the *V*-band and the sample of 92 LMC Cepheids (Persson et al. 2004) for the test in the *K*-band. The latter is the largest observed sample of Cepheids in the near-infrared bands. For each extraction a linear regression was performed to derive the slope and the zero point of the resulting PL relation. Also, we calculated the magnitude residuals $\delta(M_V)$ and $\delta(M_K)$ as defined above for the actual observed programme stars. We have, then, compared these quantities with those derived for the whole sample in order to estimate the error due to random sampling and to optimize the number of bins we can divide our sample into. It is worth noticing here that this procedure will somewhat *overestimate* the sampling error. This is because some of the random extractions will generate a subsample that covers a small range of periods, while we have carefully selected our sample in order to cover a broad period range.

After performing 1 million extractions in each of the bands, *V* and *K*, for several bin sizes, we have settled for two metallicity bins of about 30 stars each. With this choice, $\delta(M_V)$ results to being less that 0.1 mag in 95% of the cases and never larger than 0.15. The mean value of the distribution is 0.03 mag. These results imply that the non-zero result for the high metallicity bin in Fig. 8 cannot be due to insufficient sampling of the PL relation.

As for the *K* band, the simulations indicate that $\delta(M_K)$ is smaller that 0.04 mag in 95% of the cases and never larger than 0.06 mag, with a mean of 0.01 mag. Also in this case, then, the
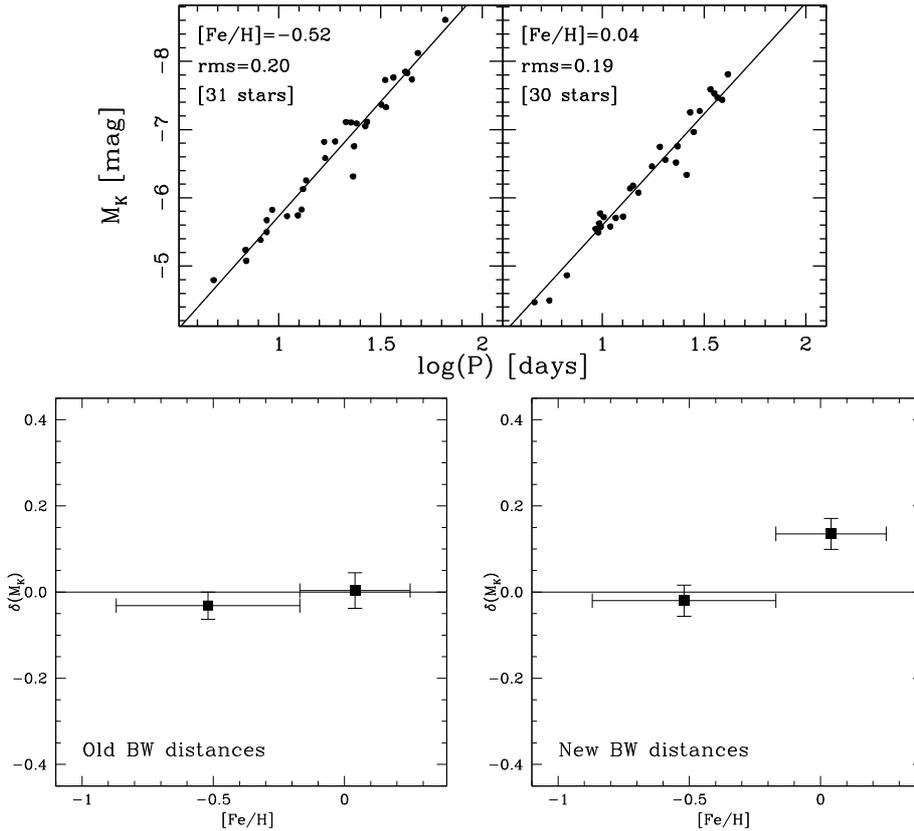
Fig. 9. *The top panels* show the PL relations calculated in each bin for the K band. The bottom panels show the residuals $\delta(M_V)$ as a function of the iron abundance for both the "Old" and the "New" Galactic Cepheid distances. The mean values of $\delta(M_K)$ in each metallicity bin are plotted as filled squares, with the vertical error-bars representing its associated error. The horizontal bars indicate the dimension of the bins. The horizontal solid lines indicate the null value which corresponds to an independence of the PL relation from the iron content.

results discussed above and displayed in Fig. 9 are not significantly affected by sampling errors.

5.2. Comparison with previous results

We compare our results with two different behaviours (see Fig. 10) as examples of the effects of the metallicity on the PL relation currently available in the literature: independence from the iron content and a monotonic decreasing trend (e.g. Kennicutt et al. 1998; Sakai et al. 2004; Storm et al. 2004; Groenewegen et al. 2004; Macri et al. 2006; Sandage & Tammann 2008), in the sense that metal-rich Cepheids are brighter than metal-poor ones.

We use for the comparison the classical results of Kennicutt et al. (1998) adopted by the HST Key Project to determine extragalactic distances with Cepheids (Freedman et al. 2001). They have analysed two Cepheid fields in M 101, with average values of metallicity around -0.4 dex and 0.28 dex (determined from measurements of oxygen in H II regions in the two fields). They have observed 29 Cepheids in the outer field (low metallicity) and 61 Cepheids in the inner field (high metallicity) with periods between 10 and 60 days. Considering the outcome of our simulations, the two Cepheid samples observed by Kennicutt and collaborators are comparable to our sub-samples in each bin, it is then reasonable to compare the qualitative indications about the effect of the metallicity that can be derived from the two analyses. The complete comparison is possible only in the V-band.

As we have already mentioned the error due to the sampling of the PL relation is much smaller than the one on the residuals. Data plotted in Figs. 8–10 disclose several circumstantial evidence. This means that the increasing trend of the latter in the V-band, as a function of the iron content, is real with a confidence level of 99%.
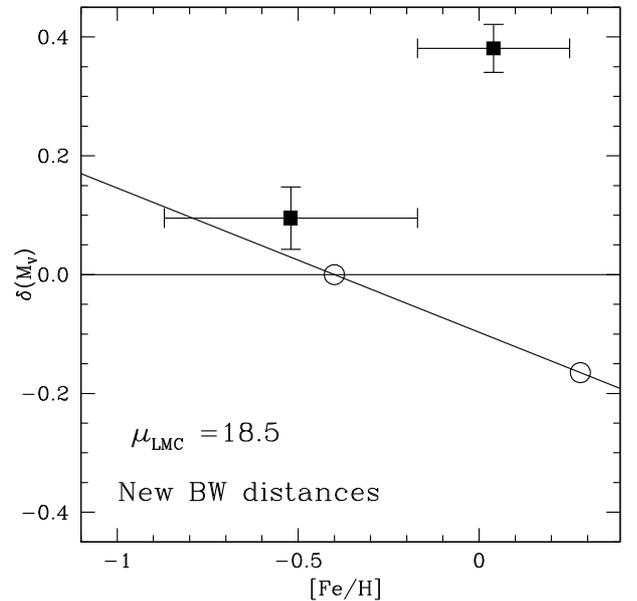
Fig. 10. The V-band residuals compared to Freedman et al. (2001) PL relation are plotted against the iron content measured from observed spectra (*bottom right panel* in Fig. 8). The filled squares display the mean value in each metallicity bin, with its associated errorbar. The metallicity dependence estimated by Kennicutt et al. (1998) using two Cepheid fields in M 101 (open circles) is shown as a full line.

i) V-band case

– *No dependence of $\delta(M_V)$ on [Fe/H]*: a null effect on the metal abundance would imply that the residuals of the two bins should be located, within the errors, along the independence line. Current findings and the outcome of the
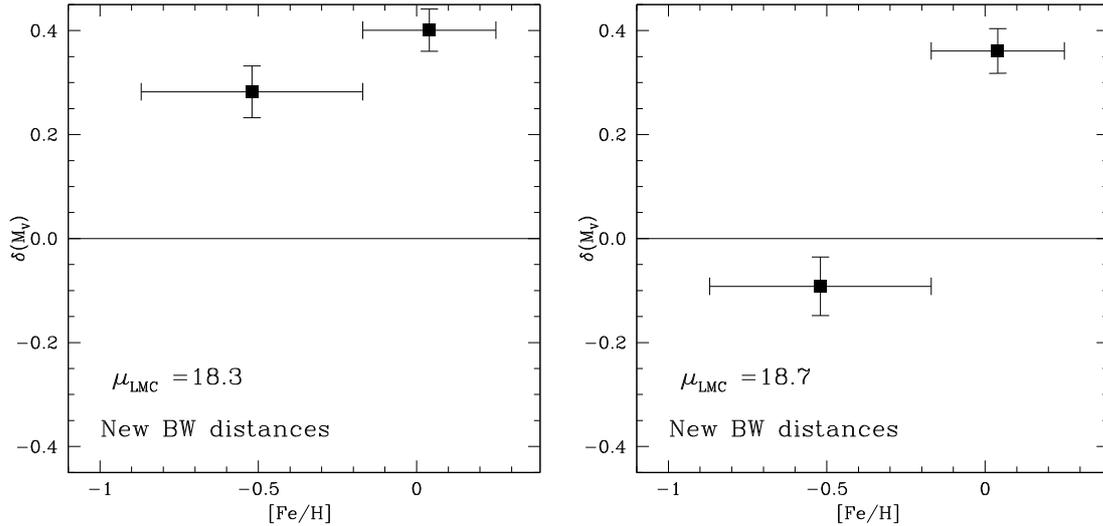
Fig. 11. The V-band residuals compared to the Freedman et al. (2001) PL relation versus the iron content measured from observed spectra, assuming an LMC distance modulus of 18.3 (*left*) and of 18.7 (*right*). The filled squares represent the mean value in each metallicity bin, with its associated errorbar.

simulations mentioned above indicate that this hypothesis can be excluded completely. The increasing trend of the residual in the V-band, as a function of the iron content, is real with a confidence level larger than 95%.

– *Monotonically decreasing $\delta(M_V)$*: we compare the classical results of Kennicutt et al. (1998, open circles and solid line in Fig. 10) with our data. Since the increasing trend of our residuals is real, this hypothesis is incompatible with our results. In passing, we also note that the reddening estimates adopted by Kennicutt et al. (1998) are based on the observed mean colors. However, metal-poor Cepheids are, at fixed period, hotter than metal-rich ones. Therefore, Kennicutt et al. would have underestimated the reddenings and the luminosities of his metal-poor sample, producing an apparent under-luminosity for metal-poor Cepheids.

ii) K-band case

– Current data do not allow us to reach a firm conclusion concerning the metallicity effect.

To summarize, we found an increasing trend of the V-band residuals with the iron content. This result is in disagreement with an independence of the PL relation on iron abundance and with the linearly decreasing trend found by other observational studies in the literature (e.g. Kennicutt et al. 1998).

5.3. LMC distance: "short" scale vs. "long" scale

Regrettably we can find in the recent literature values of the LMC distance modulus ranging from 18.1 to 18.8, not always obtained with different techniques. Those studies finding a distance modulus less than 18.5 support the so-called "short" distance scale, whereas those finding it greater than 18.5 support the "long" distance scale (for a review of the results and methods see Benedict et al. 2002; Gibson 2000). More recently, Schaefer (2008) found that distance estimates to the LMC published before 2001 present a large spread ($18.1 \leq \mu \leq 18.8$). On the other hand, distances published after 2002 tightly concentrate around the value adopted by the HST Key Projects ($\mu = 18.5$, Freedman et al. 2001; Saha et al. 2006). In order to overcome this suspicious bias, we decided to investigate the different behaviour of

the PL relation depending on the adopted LMC distance scale. In order to do that, we have repeated our calculation of the V-band residuals assuming a distance modulus for LMC of 18.3 (representative of the "short" scale) and of 18.7 (for the "long" scale). The results are shown in Fig. 11.

In the left and right panel, the V-band residuals refer to the "short" and the "long" distance scale, respectively. For $\mu_{\rm LMC}$ of 18.3, the V-band residuals are located at least at 5σ from zero. The difference between the metal-poor and the metal-rich bin is of the order of one σ. This trend is similar to the trend we obtained using $\mu_{\rm LMC} = 18.5$, however, the distance from zero of the metal-poor bin is significantly larger. This result disagrees with an independence of the PL relation on the iron abundance and the monotonic decreasing behaviour at the 99.99% level (according to the χ^2 method). On the other hand, the $\delta(M_V)$ values for $\mu_{\rm LMC}$ of 18.7 are located at ≈ 2 (metal-poor) and ~ 8 (metal-rich) σ from zero. The difference between the two bins is at least at 4σ level. The data trend is slightly steeper than for $\mu_{\rm LMC} = 18.5$. Using again a χ^2 technique, we find that this result disagrees with an independence of the PL relation on iron abundance and with the linearly decreasing trend often quoted in the literature (e.g. Kennicutt et al. 1998).

The results based on the tests performed assuming different LMC distances are the following:

Short scale – data plotted in the left panel of Fig. 11 indicate that V-band PL relation does depend on the metal content. Indeed, the two bins are located at least at 5σ from zero. This means that the zero-point of the quoted PL relations do depend on the metal abundance. However, the difference between the two bins is small and of the order of one σ. This indicates that the metallicity effect supported by the short scale is mainly caused by a difference in the zero-point. This result would imply a significant difference in the zero-point of Magellanic Cepheids. However, such a difference is not supported by current empirical (Laney & Stobie 2004; van Leeuwen et al. 2007; Fouqué et al. 2007; Sandage & Tammann 2008) and theoretical evidence.

Long scale – data plotted in the right panel of Fig. 11 indicates that V-band PL relation does depend on the metal content. The difference from zero ranges from ~ 2 for the metal-poor bin to more than 8σ for the metal-rich bin. Moreover, the two

bins differ at 4.5σ level. This means that the metallicity effect supported by the long scale is mainly caused by a difference in the slope. This finding, taken at face value, would imply that metal-poor Cepheids (e.g. Cepheids in IC 1613, $-1.3 \leq$ [Fe/H] ≤ -0.7, Skillman et al. 2003) should be, at fixed period, ≈ 0.5 (V) mag brighter than Galactic Cepheids. This difference is not supported by current empirical (Dolphin et al. 2003; Antonello et al. 2006; Pietrzynski et al. 2006; Saha et al. 2006; Fouqué et al. 2007) and theoretical evidence.

The quoted results suggest that the V-band PL relation is affected by metal abundance. This finding is marginally affected by the adopted LMC distance. It is worth mentioning that recent empirical estimates based on robust primary standard candles indicate that the true LMC distance is 18.5 ± 0.1 (Alves 2004; Benedict et al. 2007; van Leeuwen et al. 2007; Catelan & Cortes 2008; Feast et al. 2008; Groenewegen et al. 2008; Sollima et al. 2008). In view of this convergence on the LMC distance and on the results based on the "short" and on the "long" distance scale, the results based on $\mu_{\rm LMC} = 18.5$ appear to be the most reliable ones.

6. Conclusions

We have directly measured the iron abundances for 68 Galactic and Magellanic Cepheids from FEROS and UVES high resolution and high signal-to-noise spectra. We have used these measurements to assess the influence of the stellar iron content on the Cepheid PL relation in the V and in the K band. In order to do this we have related the V-band and the K-band residuals from the standard PL relations of Freedman et al. (2001) and Persson et al. (2004), respectively, to [Fe/H]. Differently from previous studies, we can constrain the PL relation using Cepheids with known distance moduli and chemical abundances, homogeneously measured, that cover almost a factor of ten in metallicity.

For our Galactic sample, we find that the mean value of the iron content is solar ($\sigma = 0.10$, see Fig. 6), with a range of values between -0.18 dex and $+0.25$ dex. For the LMC sample, we find that the mean value is about ~ -0.33 dex ($\sigma = 0.13$, see Fig. 6), with a range of values between -0.62 dex and -0.10 dex. For the SMC sample, we find that the mean value is about ~ -0.75 dex ($\sigma = 0.08$, see Fig. 6), with a range of values between -0.87 and -0.63.

We have compared our results with the analyses of FC97, Andrievsky et al. (2002a,b,c) and Luck et al. (2003) for the Galactic Cepheids and LL92 and L98 for the Magellanic Clouds. Regarding the Galactic sample, our results are marginally more in agreement with Andrievsky's values than with FC97 and the differences, on average, appear rather small. Considering the Magellanic Cepheids, we have a poor agreement with LL92, which could be in part accounted for by different analytical tools and data quality. Our data are in better agreement with L98 results and the spread of our iron abundances in the LMC and SMC is similar to the one they reported. We note that the mean metallicity that they found with their complete sample (-0.30 dex and -0.74 dex) is in very good agreement with our results.

Our main results concerning the effect of the iron abundance on the PL relation are summarized in Figs. 8 and 9 (bottom panels) and they hold for a LMC distance modulus of 18.50. In Fig. 10 is also showed the comparison in the V-band with the empirical results of Kennicutt et al. (1998) in two Cepheid fields of M 101 (open circles and solid line). The main findings can be summarized as follows:

– The V-band PL relation does depend on the metal abundance. This finding is marginally affected by the adopted distance scale for the Galactic Cepheids and by the LMC distance.
– Current data do not allow us to reach a firm conclusion concerning the dependence of the K-band PL relation on the metal content. The use of the most recent distances for Galactic Cepheids (Benedict et al. 2007; Fouquè et al. 2007; van Leeuwen et al. 2007) indicates a mild metallicity effect. On the other hand, the use of the old distances (Storm et al. 2004) suggest a vanishing effect.
– Residuals based on a canonical LMC distance ($\mu_{\rm LMC} = 18.5$) and on the most recent distances for Galactic Cepheids present a well defined effect in the V-band. The metal-poor and the metal-rich bin are $\approx 2\sigma$ and $\approx 9\sigma$ from the null hypothesis. Moreover, the two metallicity bins differ at the 3σ level.
– By assuming a "short" LMC distance ($\mu_{\rm LMC} = 18.3$) the residuals present a strong metallicity dependency in the zero-point of the V-band PL relation. By assuming a "long" LMC distance ($\mu_{\rm LMC} = 18.7$) we found a strong metallicity effect when moving from metal-poor to metal-rich Cepheids. This indicates a significant change in the slope and probably in the zero-point. The findings based on the "short" and on the "long" LMC distance are at odds with current empirical and theoretical evidence, suggesting a smaller metallicity effect.
– Metal-rich Cepheids in the V-band are systematically fainter than metal-poor ones. This evidence is strongly supported by the canonical, the "short" and the "long" LMC distance.

The above results together with recent robust LMC distance estimates indicate that the behaviours based on the canonical distance appear to be the most reliable ones.

In order to constrain on a more quantitative basis the metallicity dependence of both zero-point and slope of the optical PL relations is required a larger number of Cepheids covering a broader range in metal abundances. Moreover, for each metallicity bin Cepheids covering a broad period range are required to reduce the error on the residuals and to constrain on a quantitative basis the fine structure of the PL relation in optical and NIR photometric bands.

References

Alves, D. 2004, NewAR, 48, 659
Andrievsky, S. M., Kovtyukh, V. V., Korotin, S. A., et al. 2001, A&A 367, 605
Andrievsky, S. M., Kovtyukh, V. V., Luck, R. E., et al. 2002a, A&A, 381, 32

Andrievsky, S. M., Bersier, D., Kovtyukh, V. V., et al. 2002b, A&A, 384, 140
Andrievsky, S. M., Kovtyukh, V. V., Luck, R. E., et al. 2002c, A&A 392, 491
Andrievsky, S. M., Luck, R. E., Martin, P., & Lepine, J. R. D. 2004, A&A, 413, 159
Antonello, E., Fossati, L., Fugazza, D., Mantegazza, L., & Gieren, W. 2006, A&A, 445, 901
Baraffe, I., & Alibert, Y. 2001, A&A, 371, 592
Benedict, G. F., McArthur, B. E., Fredrick, L. W., et al. 2002, AJ, 123, 473
Benedict, G. F., McArthur, B. E., Feast, M. W., et al. 2007, AJ, 133, 1810
Bono, G., Caputo, F., Castellani, V., & Marconi, M. 1999, ApJ, 512, 711
Bono, G., Caputo, F., Fiorentino, G., et al. 2008, ApJ, accepted [arXiv:0805.1592]
Borissova, J., Minniti, D., Rejkuba, M., et al. 2004, A&A, 423, 97
Caputo, F. 2008, Mem Sait, in press
Caputo, F., Marconi, M., Musella, I., & Santolamazza, P. 2000, A&A, 359, 1059
Carpenter, J. M. 2001, AJ, 121, 2851
Castelli, F., & Kurucz, R. L. 2003, in Modelling of Stellar Atmospheres, ed. N. Piskunov, W. W. Weiss, & D. F. Gray (San Francisco: ASP), IAU Symp., 210, 841
Castelli, F., Gratton, R. G., & Kurucz, R. L. 1997, A&A, 318, 841
Catelan, M., & Cortés, C. 2008, ApJ, 676, 135
Cayrel, R. 1988, in The Impact of Very High S/N Spectroscopy on Stellar Physics (Dordrecht: Kluwer Academic Publishers), IAU Symp., 132, 345
Charbonneau, P. 1995, ApJS, 101, 309
Chiosi, C., Wood, P., Bertelli, G., & Bressan, A. 1992, ApJ, 387, 320
Ciardullo, R., Feldmeier, J. J., Jacoby, G. H., et al. 2002, ApJ, 577, 31
Cioni, M.-R. L., van der Marel, R. P., Loup, C., & Habing, H. J. 2000, A&A, 359, 601
Clementini, G., Carretta, E., Gratton, R., et al. 1995, AJ, 110, 2319
Dekker, H., D'Odorico, S., Kaufer, A., et al. 2000, SPIE, 4008, 534
Dìaz, A. I., Castellanos, M., Terlevich, E., & Luisa Garcìa-Vargas, M. 2000, MNRAS, 318, 462
Dolphin, A. E., Saha, A., Skillman, E. D., et al. 2003, AJ, 125, 1261
Feast, M. W., & Catchpole, R. M. 1997, MNRAS, 286, L1
Feast, M. W., Laney, C. D., Kinman, T. D., van Leeuwen, F., & Whitelock, P. A. 2008 [arXiv:0803.0466]
Fernie, J. D., Evans, N. R., Beattie, B., & Seager, S. 1995, IBVS, 4148, 1
Fiorentino, G., Caputo, F., Marconi, M., & Musella, I. 2002, ApJ, 576, 402
Fouqué, P., & Gieren, W. P. 1997, A&A, 320, 799
Fouqué, P., Arriagada, P., Storm, J., et al. 2007, A&A, 476, 73
Freedman, W. L., & Madore, B. F. 1990, ApJ, 365, 186
Freedman, W. L., Madore, B. F., Gibson, B. K., et al. 2001, ApJ, 553, 47
Fry, A. M., & Carney, B. W. 1997, AJ, 113, 1073 (FC97)
Fuhr, J. R., Martin, G. A., & Wiese, W. L. 1988, J. Phys. & Chem. Ref. Data, 17, Suppl., 4
Gibson, B. K. 2000, MmSAI, 71, 693
Gould, A. 1994, ApJ, 426, 542
Gratton, R., Sneden, C., & Carretta, E. 2004, ARA&A, 42, 385
Gray, D. F. 1994, PASP, 106, 1248
Grevesse, N., & Sauval, A. J. 1998, SSRv, 85, 161
Grocholski, A. J., Cole, A. A., Sarajedini, A., Geisler, D., & Smith, V. V. 2006, AJ, 132, 1630
Groenewegen, M. A. T. 2004, MNRAS, 353, 903
Groenewegen, M. A. T. 2007, A&A, A&A, 474, 975
Groenewegen, M. A. T. 2008, A&A, accepted
Groenewegen, M. A. T., Romaniello, M., Primas, F., & Mottini, M. 2004, A&A, 420, 655
Groenewegen, M. A. T., Udalski, A., & Bono, G. 2008, A&A, 481, 441
Gustafsson, B., Bell, R. A., Eriksson, K., & Nordlund, A. 1975, A&A, 42, 407
Herrnstein, J. R., Moran, J. M., Greenhill, L. J., & Trotter, A. S. 2005, ApJ, 629, 719
Hill, V. 1997, A&A, 324, 435
Hill, V., Andrievsky, S. M., & Spite, M. 1995, A&A, 293, 347
Kaufer, A., D'Odorico, S., & Kaper, L. 2004, UVES User Manual, Issue 1.9, VLT-MAN-ESO-13200-1825
Kennicutt, R. C., Stetson, P. B., Saha, A., et al. 1998, ApJ, 498, 181

Kervella, P., Bersier, D., Mourard, D., et al. 2004, A&A, 428, 587
Kiss, L. L., & Vinko, J. 2000, MNRAS, 314, 420
Kochanek, C. S. 1997, ApJ, 491, 13
Koen, C., Marang, F., Kilkenny, D., & Jacobs, C. 2007, MNRAS, 380, 1433
Korn, A. J., Becker, S. R., Gummersbach, C. A., & Wolf, B. 2000, A&A, 353, 655
Kovtyukh, V. V., & Gorlova, N. I. 2000, A&A, 351, 597
Kovtyukh, V. V., Andrievsky, S. M., Belik, S. I., & Luck, R. E. 2005a, AJ, 129, 433
Kovtyukh, V. V., Wallerstein, G., & Andrievsky, S. M. 2005b, PASP, 117, 1173
Kupka, F., Piskunov, N. E., Ryabchikova, T. A., Stempels, H. C., & Weiss W. W. 1999, A&AS, 138, 119
Kurucz, R. L. 1993, CD-ROMS #1, 13, 18
Laney, C. D., & Caldwell, J. A. R. 2007, MNRAS, 377, 147
Laney, C. D., & Stobie, R. S. 1992, A&AS, 93, 93
Laney, C. D., & Stobie, R. S. 1994, MNRAS, 226, 441
Laney, C. D., & Stobie, R. S. 1995, MNRAS, 274, 337
Lemasle, B., François, P., Bono, G., et al. 2007, A&A, 467, 283
Luck, R. E., & Andrievsky, S. M. 2004, AJ, 128, 343
Luck, R. E., & Lambert, D. L. 1981, ApJ, 245, 1018
Luck, R. E., & Lambert, D. L. 1985, ApJ, 298, 872
Luck, R. E., & Lambert, D. L. 1992, ApJS, 79, 303 (LL92)
Luck, R. E., Moffet, T. J., Barnes, T. G. III, & Gieren, W. P. 1998, AJ, 115, 605 (L98)
Luck, R. E., Gieren, W. P., Andrievsky, S. M., et al. 2003, A&A, 401, 939
Macri, L. M., Stanek, K. Z., Jr., Bersier, D., Greenhill, L. J., & Reid, M. J. 2006, ApJ, 652, 1133
Marconi, M., Musella, I., & Fiorentino, G. 2005, ApJ, 632, 590
Pel, J. W. 1978, A&A, 62, 75
Persson, S. E., Madore, B. F., Krzeminski, W., et al. 2004, AJ, 128, 2239
Pietrzyński, G., Gieren, W., Soszyński, I., et al. 2006, ApJ, 642, 216
Pompéia, L., Hill, V., Spite, M., et al. 2008, A&A, 480, 379
Pritchard, J. D. 2004, FEROS-II User Manual, Issue 1.4, LSO-MAN-ESO-22200-0001
Rolleston, W. R. J., Dufton, P. L., Fitzsimmons, A., et al. 1993, A&A, 277, 10
Rolleston, W. R. J., Trundle, C., & Dufton, P. L. 2002, A&A, 396, 53
Romaniello, M., Primas, F., Mottini, M., et al. 2005, A&A, 429, L37 (Paper I)
Russell, S. C., & Bessell, M. S. 1989, ApJS, 70, 865
Russell, S. C., & Dopita, M. A. 1992, ApJ, 384, 508
Ryabchikova, T. A. Piskunov, N. E., Stempels, H. C., Kupka, F., & Weiss, W. W. 1999, proc. of the 6th International Colloquium on Atomic Spectra and Oscillator Strengths, Victoria BC, Canada, 1998, Phys. Scr., T83, 162
Saha, A., Thim, F., Tammann, G. A., et al. 2006, ApJS, 165, 108
Sakai, S., Ferrarese, L., Kennicutt, R. C., & Saha, A. 2004, ApJ, 608, 42
Sandage, A., & Tamman, G. A. 2008 [arXiv:0803.3836]
Sandage, A., Bell, R. A., & Tripicco, M. J. 1999, ApJ, 522, 250
Sasselov, D. D., Beaulieu, J. P., Renault, C., et al. 1997, A&A, 324, 471
Schaefer, B. E. 2008, AJ, 135, 112S
Skillman, E. D., Tolstoy, E., Cole, A. A., et al. 2003, ApJ, 596, 253
Sneden, C. 1973, ApJ, 184, 839
Sollima, A., Cacciari, C., Arkharov, A. A. H., et al. 2008, MNRAS, 384, 1583
Storm, J., Carney, B. W., Gieren, W. P., et al. 2004, A&A, 415, 531
Szabados, L. 2003, Inf. Bull. Var. Stars, 5394
Sziládi, K., Vinkó, J., Poretti, E., Szabados, L., & Kun, M. 2007, A&A, 473, 579
Tammann, G. A., Sandage, A., & Reindl, B. 2007 [arXiv:0712.2346]
Trundle, C., Dufton, P. L., Hunter, I., et al. 2007, A&A, 471, 625
Turner, D. G., & Burke, J. F. 2002, AJ, 124, 2931
Van Leeuwen, F., Feast, M. W., Whitelock, P. A., & Laney, C. D. 2007, MNRAS, 379, 723
Udalski, A., Soszynski, I., Szymanski, M., et al. 1999, AcA, 49, 437
Udalski, A., Wyrzykowski, L., Pietrynski, G., et al. 2001, Acta Astron., 51, 221
Walker, A. R. 2003, in: Stellar candles for the extragalactic distance scale, Lect. Notes Phys., 635, 265
Westerlund, B. E. 1997, in The Magellanic Clouds, Cambridge Astrophys. Ser., 29
Zaritsky, D., Kennicutt, R. C., Jr., & Huchra, J. P. 1994, ApJ, 420, 87

Table 4. Complete line list with wavelength, ion identification, excitation potential (*EP*) and log g_f values.

Table 4. continued.

λ [Å]	Ion	EP	log g_f
4892.87	Fe I	4.22	−1.34
4917.23	Fe I	4.19	−1.29
4924.77	Fe I	2.28	−2.24
4932.08	Fe I	4.65	−1.49
4950.10	Fe I	3.42	−1.67
4973.11	Fe I	3.96	−0.95
4994.13	Fe I	0.91	−3.08
5029.62	Fe I	3.41	−2.05
5044.21	Fe I	2.85	−2.04
5049.82	Fe I	2.28	−1.36
5054.64	Fe I	3.64	−1.92
5056.84	Fe I	4.26	−1.96
5067.15	Fe I	4.22	−0.97
5072.67	Fe I	4.22	−0.84
5083.34	Fe I	0.96	−2.96
5090.77	Fe I	4.26	−0.40
5126.19	Fe I	4.26	−1.08
5133.69	Fe I	4.18	0.14
5171.60	Fe I	1.48	−1.79
5198.72	Fe I	2.22	−2.14
5215.18	Fe I	3.27	−0.87
5216.28	Fe I	1.61	−2.15
5217.40	Fe I	3.21	−1.07
5242.49	Fe I	3.63	−0.97
5243.78	Fe I	4.26	−1.15
5257.65	Fe I	3.57	−2.79
5281.80	Fe I	3.04	−0.83
5288.52	Fe I	3.69	−1.51
5307.37	Fe I	1.61	−2.99
5324.18	Fe I	3.21	−0.10
5326.14	Fe I	3.57	−2.07
5339.93	Fe I	3.27	−0.65
5364.87	Fe I	4.45	0.23
5365.40	Fe I	3.57	−1.02
5367.47	Fe I	4.42	0.44
5373.71	Fe I	4.47	−0.86
5379.57	Fe I	3.69	−1.51
5383.37	Fe I	4.31	0.65
5389.49	Fe I	4.41	−0.57
5391.46	Fe I	4.15	−0.78
5393.18	Fe I	3.24	−0.72
5398.28	Fe I	4.45	−0.67
5405.78	Fe I	0.99	−1.84
5410.91	Fe I	4.47	0.40
5415.20	Fe I	4.39	0.64
5417.04	Fe I	4.41	−1.42
5424.07	Fe I	4.32	0.52
5434.53	Fe I	1.01	−2.22
5445.04	Fe I	4.39	−0.02
5452.09	Fe I	3.64	−2.86
5464.28	Fe I	4.14	−1.40
5466.40	Fe I	4.37	−0.63
5497.52	Fe I	1.01	−2.85
5501.46	Fe I	0.96	−3.05
5506.78	Fe I	0.99	−2.80
5522.45	Fe I	4.21	−1.47
5531.98	Fe I	4.91	−1.61
5543.15	Fe I	3.69	−1.57
5554.89	Fe I	4.54	−0.44
5560.22	Fe I	4.43	−1.10
5561.24	Fe I	4.61	−1.21
5562.71	Fe I	4.44	−0.66
5565.71	Fe I	4.61	−0.21
5568.62	Fe I	3.41	−0.49
5572.84	Fe I	3.40	−0.27

λ [Å]	Ion	EP	log g_f
5576.09	Fe I	3.43	−1.00
5584.76	Fe I	3.57	−2.32
5586.77	Fe I	3.37	−0.10
5633.97	Fe I	4.99	−0.23
5635.85	Fe I	4.26	−1.52
5638.27	Fe I	4.22	−0.68
5641.46	Fe I	4.26	−0.87
5653.89	Fe I	4.39	−1.36
5658.82	Fe I	3.40	−0.85
5661.36	Fe I	4.28	−1.79
5679.02	Fe I	4.65	−0.71
5686.53	Fe I	4.55	−0.66
5691.51	Fe I	4.30	−1.46
5707.05	Fe I	3.64	−2.40
5717.85	Fe I	4.28	−0.99
5720.89	Fe I	4.55	−1.76
5731.77	Fe I	4.26	−1.08
5741.86	Fe I	4.26	−1.61
5752.01	Fe I	4.55	−0.88
5753.12	Fe I	4.26	−0.69
5762.43	Fe I	3.64	−2.30
5762.99	Fe I	4.21	−0.36
5775.07	Fe I	4.22	−1.08
5778.47	Fe I	2.59	−3.49
5793.93	Fe I	4.22	−1.60
5804.06	Fe I	3.88	−2.15
5806.73	Fe I	4.61	−0.88
5809.25	Fe I	3.88	−1.61
5814.80	Fe I	4.28	−1.82
5816.37	Fe I	4.55	−0.60
5834.02	Fe I	4.91	−0.95
5848.13	Fe I	4.61	−1.06
5852.19	Fe I	4.55	−1.14
5855.13	Fe I	4.61	−1.51
5856.08	Fe I	4.29	−1.54
5859.56	Fe I	4.55	−0.57
5862.36	Fe I	4.55	−0.26
5873.21	Fe I	4.26	−1.97
5877.77	Fe I	4.18	−2.12
5883.84	Fe I	3.96	−1.08
5902.52	Fe I	4.59	−1.74
5905.67	Fe I	4.65	−0.69
5909.99	Fe I	3.21	−2.62
5916.25	Fe I	2.45	−2.88
5927.80	Fe I	4.65	−1.01
5930.17	Fe I	4.65	−0.14
5934.66	Fe I	3.93	−1.00
5952.73	Fe I	3.98	−1.44
5956.70	Fe I	0.86	−4.52
5858.33	Fe I	2.18	−4.16
5975.35	Fe I	4.83	−0.69
5976.78	Fe I	3.94	−1.17
5983.69	Fe I	4.55	−0.58
5984.79	Fe I	4.73	−0.19
5987.05	Fe I	4.80	−0.23
5997.78	Fe I	4.61	−1.70
6003.03	Fe I	3.88	−0.89
6005.54	Fe I	2.59	−3.60
6007.96	Fe I	4.65	−0.61
6008.56	Fe I	3.88	−0.83
6012.21	Fe I	2.22	−4.04
6020.19	Fe I	4.61	−0.27
6024.07	Fe I	4.55	0.04
6027.06	Fe I	4.08	−1.10
6056.01	Fe I	4.73	−0.46
6062.89	Fe I	2.18	−3.93

Table 4. continued.

λ [Å]	Ion	EP	$\log g_f$
6065.48	Fe I	2.61	–1.53
6078.50	Fe I	4.80	–0.22
6079.02	Fe I	4.65	–0.93
6082.72	Fe I	2.22	–3.57
6085.27	Fe I	2.76	–2.86
6089.57	Fe I	5.02	–0.84
6093.66	Fe I	4.61	–1.32
6096.69	Fe I	3.98	–1.75
6127.91	Fe I	4.14	–1.39
6136.62	Fe I	2.45	–1.40
6137.70	Fe I	2.59	–1.40
6151.62	Fe I	2.18	–3.30
6157.73	Fe I	4.08	–1.18
6165.37	Fe I	4.14	–1.46
6170.49	Fe I	4.80	–0.30
6173.34	Fe I	2.22	–2.81
6180.22	Fe I	2.73	–2.65
6188.04	Fe I	3.94	–1.58
6191.57	Fe I	2.43	–1.42
6200.32	Fe I	2.61	–2.31
6213.43	Fe I	2.22	–2.55
6215.15	Fe I	4.19	–1.14
6219.28	Fe I	2.20	–2.41
6226.77	Fe I	3.88	–2.05
6229.23	Fe I	2.85	–2.85
6230.73	Fe I	2.56	–1.33
6232.65	Fe I	3.65	–1.13
6240.66	Fe I	2.22	–3.28
6246.32	Fe I	3.60	–0.63
6252.55	Fe I	2.40	–1.68
6265.13	Fe I	2.18	–2.51
6270.23	Fe I	2.86	–2.46
6301.51	Fe I	3.65	–0.58
6302.50	Fe I	3.69	–0.97
6311.51	Fe I	2.83	–3.09
6322.69	Fe I	2.59	–2.28
6330.86	Fe I	4.73	–1.14
6335.34	Fe I	2.20	–2.25
6336.84	Fe I	3.69	–0.67
6344.15	Fe I	2.43	–2.89
6355.04	Fe I	2.85	–2.32
6358.69	Fe I	0.86	–4.11
6380.75	Fe I	4.19	–1.27
6392.55	Fe I	2.28	–3.94
6393.60	Fe I	2.43	–1.58
6400.01	Fe I	3.60	–0.29
6408.01	Fe I	3.69	–1.02
6411.65	Fe I	3.65	–0.49
6419.98	Fe I	4.73	–0.17
6421.35	Fe I	2.28	–2.12
6430.85	Fe I	2.18	–2.06
6469.19	Fe I	4.83	–0.77
6475.63	Fe I	2.56	–2.94
6481.88	Fe I	2.28	–2.91
6494.98	Fe I	2.40	–1.43
6496.47	Fe I	4.79	–0.57
6498.95	Fe I	0.96	–4.62
6518.38	Fe I	2.83	–2.54
6533.97	Fe I	4.56	–1.11
6546.25	Fe I	2.76	–1.54
6569.22	Fe I	4.73	–0.42
6574.23	Fe I	0.99	–5.02
6575.04	Fe I	2.59	–2.71
6592.91	Fe I	2.73	–1.62

Table 4. continued.

λ [Å]	Ion	EP	$\log g_f$
6593.88	Fe I	2.43	–2.29
6597.61	Fe I	4.80	–0.85
6608.03	Fe I	2.28	–3.94
6609.12	Fe I	2.56	–2.61
6627.56	Fe I	4.55	–1.46
6646.93	Fe I	2.61	–1.99
6648.08	Fe I	1.01	–5.42
6677.99	Fe I	2.69	–1.37
6703.57	Fe I	2.76	–3.01
6705.10	Fe I	4.61	–1.39
6710.31	Fe I	1.49	–4.78
6713.05	Fe I	4.61	–0.96
6713.76	Fe I	4.80	–1.37
6715.38	Fe I	4.61	–1.64
6725.36	Fe I	4.10	–2.30
6726.64	Fe I	4.61	–1.01
6733.15	Fe I	4.64	–1.58
6737.99	Fe I	4.55	–1.75
6739.52	Fe I	1.56	–4.79
6750.15	Fe I	2.42	–2.58
6752.72	Fe I	4.64	–1.19
6783.70	Fe I	2.59	–3.98
6804.00	Fe I	4.65	–1.50
6806.85	Fe I	2.73	–3.09
6810.28	Fe I	4.61	–0.94
6820.43	Fe I	4.64	–1.10
6828.61	Fe I	4.64	–0.80
6837.00	Fe I	4.59	–1.69
6839.83	Fe I	2.56	–3.31
6841.35	Fe I	4.61	–0.77
6843.67	Fe I	4.55	–0.78
6855.15	Fe I	4.56	–0.57
6855.74	Fe I	4.61	–1.64
6858.16	Fe I	4.61	–0.91
6945.20	Fe I	2.42	–2.43
6951.25	Fe I	4.56	–0.89
6999.90	Fe I	4.10	–1.38
7022.98	Fe I	4.19	–1.10
7090.38	Fe I	4.23	–1.06
7093.09	Fe I	4.56	–2.02
7095.43	Fe I	4.21	–2.02
7107.46	Fe I	4.19	–1.34
7112.18	Fe I	2.99	–3.00
7127.56	Fe I	4.99	–1.36
7130.92	Fe I	4.22	–0.73
7132.99	Fe I	4.08	–1.63
7142.51	Fe I	4.96	–0.82
7145.32	Fe I	4.61	–1.53
7187.32	Fe I	4.10	–0.15
7212.43	Fe I	4.96	–0.85
7219.69	Fe I	4.08	–1.69
7382.02	Fe I	4.61	–1.42
7411.15	Fe I	4.28	–0.30
7435.59	Fe I	5.31	–0.71
7440.95	Fe I	4.91	–0.68
7443.02	Fe I	4.19	–1.82
7445.75	Fe I	4.26	–0.24
7447.39	Fe I	4.96	–1.21
7461.52	Fe I	2.56	–3.58
7491.65	Fe I	4.30	–1.01
7495.06	Fe I	4.22	–0.10
7498.53	Fe I	4.14	–2.25
7506.01	Fe I	5.06	–1.22
7507.26	Fe I	4.41	–1.48
7511.02	Fe I	4.18	0.10

Table 4. continued.

λ [Å]	Ion	EP	log g_f
7531.14	Fe I	4.37	−1.31
7547.90	Fe I	5.10	−1.35
7559.72	Fe I	5.06	−1.08
7568.89	Fe I	4.28	−0.88
7583.79	Fe I	3.02	−1.89
7586.01	Fe I	4.31	−0.87
7661.19	Fe I	4.26	−0.95
7719.04	Fe I	5.03	−1.31
7748.27	Fe I	2.95	−1.75
7751.11	Fe I	4.99	−0.75
7807.91	Fe I	4.99	−0.54
7832.20	Fe I	4.43	0.11
7855.40	Fe I	5.06	−1.02
7869.61	Fe I	4.37	−1.88
7912.87	Fe I	0.86	−4.85
4893.82	Fe II	2.83	−4.45
4923.93	Fe II	2.88	−1.35
4993.35	Fe II	2.81	−3.56
5100.66	Fe II	2.81	−4.16
5132.67	Fe II	2.81	−3.95
5197.58	Fe II	3.23	−2.23
5234.63	Fe II	3.22	−2.22
5256.94	Fe II	2.89	−4.25
5325.56	Fe II	3.22	−3.18
5362.87	Fe II	3.20	−2.62
5414.07	Fe II	3.22	−3.54
5425.26	Fe II	3.20	−3.27
5534.85	Fe II	3.24	−2.75
5627.49	Fe II	3.39	−4.01
5932.06	Fe II	3.20	−4.81
5991.37	Fe II	3.15	−3.50
6084.10	Fe II	3.20	−3.80
6113.33	Fe II	3.22	−4.12
6147.74	Fe II	3.89	−2.72
6149.25	Fe II	3.89	−2.72
6238.39	Fe II	3.87	−2.52
6247.56	Fe II	3.89	−2.33
6369.46	Fe II	2.89	−4.14
6383.72	Fe II	5.55	−2.07
6416.92	Fe II	3.89	−2.65
6432.68	Fe II	2.89	−3.69
6442.94	Fe II	5.55	−2.46
6446.40	Fe II	6.22	−2.07
6456.38	Fe II	3.90	−2.18
6516.08	Fe II	2.89	−3.45
7310.22	Fe II	3.89	−3.36
7449.34	Fe II	3.89	−3.09
7479.69	Fe II	3.89	−3.68
7515.83	Fe II	3.90	−3.55
7533.37	Fe II	3.90	−3.99
7711.44	Fe II	5.51	−3.21
7711.72	Fe II	3.90	−2.50